High-Level Control of UAV Swarms with RSSI Based Position Estimation

Märta Paulsson

LUND
UNIVERSITY

Department of Automatic Control

MSc Thesis
TFRT-6046
ISSN 0280-5316

Department of Automatic Control
Lund University
Box 118
SE-221 00 LUND
Sweden

Printed in Sweden by Tryckeriet i E-huset
Lund 2017

Abstract

Search and rescue operations can greatly benefit from the use of cooperative swarms of autonomous UAVs in order to investigate areas and collect information about the position of a missing person.

In this thesis, UAV swarm algorithms are investigated where collisions are prevented both between agent pairs and between agents and static obstacles. The swarm consists of low-cost collaborative fixed-wing aircraft with communication constraints. A decentralized swarm behavior is first developed when the system is assumed to provide accurate positions of all aircraft. Further, the agents estimate their position by the use of RSSI measurements. All agents are equipped with communication devices and broadcast radio signals and measure the received signal strength in order to estimate the distance to other swarm members. These estimates are further used to develop a multilateration algorithm, where each agent estimates its own position by using distance estimates from a minimum of three nearby agents. By adding a dynamic model of the aircraft kinematics, a more accurate estimation is provided which takes account for false position estimates.

The autonomous swarm is simulated in a 2-D environment in MATLAB. The agents make decisions in real-time, where their movements are controlled by potential fields and pheromone levels. Repulsive potentials are used to prevent collision and attractive potentials are applied to form a cluster of UAVs, such that all members stay within communication range. The swarm is also attracted to unexplored areas of the environment.

When the true UAV positions are provided, the developed potential field algorithm did show promising results in terms of controlling the swarm. No collisions occurred between agent pairs or agents and obstacles. The agents did not go out of bounds and the swarm was robust as it was able to handle the loss of individual members.

For the approach of RSSI based position estimates, further development of the swarm behavior was needed. The receiver sensitivity of the communication devices limits both the maximum distance between agents and their difference in roll angle. When individual failures occurred, or when an obstacle obstructed the path of the swarm, there was not always enough RSSI measurements available to perform the multilateration algorithm. In combination with the dynamic model of the aircraft kinematics, the resulting algorithm produced position estimates with a mean error of approximately 9 meters. No significant difference was found regarding the efficiency of scanning the area when the positions were estimated by RSSI values compared to when the positions were known. However, victims may go undetected when using estimated positions if the position error results in UAVs believing they have visited certain areas they have not yet scanned.

Acknowledgements

Several people have contributed with technical expertise, practical solutions and valuable opinions throughout this thesis. Without their participation and input, the project would not have been successfully accomplished.

Firstly, I would like to thank my advisors at Saab AB, Magnus Blomberg and Lars Rundqwist, for your help, excellent ideas and feedback along the way. I would specifically like to thank Blomberg for suggesting this project and making sure I was given all the help and support needed. I also show appreciation to him for introducing me to other employees at Saab who in turn helped me design and 3-D print parts needed for taking measurements, as well as giving me access to soldering equipment. When problems arose along the way, I was supplied with suggestions on how to improve both the code and the developed solution in general.

I would like to thank Rundqwist for providing great technical insight on how to make improvements to the project, and to his expertise concerning UAVs and aircraft kinematics.

Secondly, my advisor at Lund University, Prof. Bo Bernhardsson has contributed with great ideas and advice on topics of a more technical nature. I would like to thank both Rundqwist and Bernhardsson for taking their time to read this report and providing suggestions on improvements of my thesis. Your help has been most appreciated.

I am also grateful to my examiner, Prof. Karl-Erik Årzén, for contributing with valuable feedback on my thesis report.

Special thanks go to Tina Erlandsson and Zoran Sjanic at Saab for good discussions and valuable feedback at demo forums during the semester.

I would also like to thank all the other employees at Saab who were involved or showed interest in my project.

Lastly, a shout-out to my dad, Mattias Paulsson, for helping me design and build the holder for the servo motor and rotating microcontroller, as well as assisting me while taking measurements.

To all, thank you!

Contents

List of Figures

List of Tables

Acronyms and Abbreviations

AP	Access Point
API	Application Programming Interface
CDF	Cumulative Distribution Function
DOF	Degrees of Freedom
DR	Dead Reckoning
EKF	Extended Kalman filter
FW	Fixed-Wing
GNSS	Global Navigation Satellite System
GPS	Global Positioning System
IDE	Integrated Development Environment
IEEE	Institute of Electrical and Electronics Engineers
KF	Kalman Filter
LNSM	Log-Normal Shadowing Model
LOS	Line-of-Sight
LS	Least Square
MEMS	Micro-Electro-Mechanical System
NED	North East Down
OSI	Open Systems Interconnection
PC	Personal Computer
PCB	Printed Circuit Board
PDF	Probability Density Function
PF	Particle Filter
PIO	Pigeon-Inspired Optimization
PSO	Particle Swarm Optimization
PWM	Pulse Width Modulation
RF	Radio Frequency
RRT	Rapidly Exploring Random Trees
RSS	Received Signal Strength

RSSI	Received Signal Strength Indicator
RTT	Round Trip Time
RW	Rotary-Wing
SAR	Search and Rescue
SI	Swarm Intelligence
SLAM	Simultaneous Localization and Mapping
SN	Sensor Networks
TDOA	Time Difference of Arrival
TOA	Time of Arrival
TOF	Time of Flight
TOT	Time of Transmission
UART	Universal Asynchronous Receiver/Transmitter
UAS	Unmanned Aircraft Systems
UAV	Unmanned Aerial Vehicle
WNLS	Weighted Nonlinear Least Square
WPAN	Wireless Personal Area Network
WSN	Wireless Sensor Network

1

Introduction

Search and rescue (SAR) operations are often tedious and may run under extreme conditions. Unmanned aerial vehicles (UAVs) can provide critical support as they are agile, fast, and able to perform operations that are hard, or even impossible, to execute by human operators. A UAV is an aircraft designed to operate without a human pilot on board and can be autonomous, semi-autonomous, or controlled remotely by an operator. When searching for a missing person, sensors generally have a higher success rate at low altitudes, and using manned aircraft at these altitudes may introduce too high risks. The ability to design small-sized unmanned aircraft makes them suitable to be used where small turning radius is required, such as in narrow, obstructed areas. During natural catastrophes and nuclear breakdowns, UAVs may be considered for SAR applications, especially if the area is toxic to humans and therefore dangerous for manned search operations. In a typical SAR scenario, UAVs are deployed in an area of interest and perform necessary sensory operations to collect evidence of the presence of victims. The information is thereafter reported to a remote ground station or to a rescue team.

This Master's thesis investigates swarm control algorithms for unmanned aerial vehicles (UAVs) and exhibits the compatibility of aerial SAR operations.

UAVs used in military applications are generally equipped with powerful cameras, precise global positioning systems, and long-range wireless communication devices. However, there are limitations in the use of small UAVs for civilian purposes. These aircraft obtain restrictions and limitations regarding the weight of the payload, the power, the wireless communication range, etc. However, several research studies recommend the use of applications based on swarm techniques and cooperation between aircraft, particularly for surveillance [Jaimes et al., 2008] and search missions [Varela et al., 2011].

In most outdoor environments, the Global Navigation Satellite System (GNSS) provides localization by using GPS signals. These systems require signal connections to satellites in order to operate and in obstructed areas the signals may be reflected and absorbed by different objects. This results in a positioning error, i.e. the position accuracy worsens near buildings and obstacles, such as bridges, mountains, and trees, due to satellite signal blockage or reflections and absorption. This thesis considers the use of wireless personal area network (WPAN) measurements to obtain position estimates of the swarm members. More specifically, to limit the costs of the devices involved in the positioning operations, an approach based on received radio signal strength (RSS) measurements is considered. The UAVs are assumed to be equipped with communication devices, which allow them to communicate with each other in order to improve their cooperation abilities.

This chapter discusses the use of UAVs, UAV configurations, and swarm intelligence; followed by previous work within these fields. The goal of the thesis is presented as well as the delimitation and challenge of the project. Further, the platform and hardware used are described briefly and the chapter is finalized by the outline of the report.

1.1 Background

This section presents background theory regarding UAVs, UAV configurations, swarm intelligence, and control architectures. UAV configurations refer to different categories of UAVs in terms of size, payload, range, and whether they consist of fixed or rotary wings. Control architecture refers to different architectures of swarm behavior, i.e. centralized and decentralized control.

Unmanned Aerial Vehicles

Modern UAVs are capable of performing autonomous flight missions without any interaction with a human pilot, as they are equipped with data processor units, sensors, automatic control, and communication systems. Unmanned aircraft systems (UAS) are playing increasingly prominent roles in both defense programs and civilian applications around the world. Technology advancements have enabled the development of both large unmanned aircraft and smaller, increasingly capable unmanned aircraft. The terminology *unmanned aircraft system* refers not only to the aircraft, but also to all of the supporting equipment used in the system; including sensors, microcontrollers, software, ground station computers, user interfaces, and communication hardware. In recent years, thanks to the low-cost of deploying and maintaining a UAV system, and the possibility to operate them in areas inaccessible or dangerous for human pilots, UAVs have attracted much research attention both in the military field and in civilian applications. A vast majority of UAS research is within military applications. However, the use of UAS in civilian applications, such as for search and rescue operations, has increased lately.

UAVs have already demonstrated their benefit in search and rescue operations. Hazardous environments can be avoided by human responders by deploying unmanned aircraft in these areas. In 2005, in the aftermath of Hurricane Katrina, two UAVs surveyed the damaged area in the search for trapped survivors [NSF, 2005]. UAVs were also deployed in Lushan, China, in 2013 when the city experienced an earthquake of magnitude 7.0. This work is presented in [Qi et al., 2015], where rotary-wing UAVs were implemented for rapid search and post-seismic evaluation. Over the past decade, China has been using UAVs to navigate in disaster areas to find survivors.

The potential and growing desire of using UAVs for search and rescue applications is supported by an increasing number of work in the areas of image recognition for victim detection, path planning, and task allocation [Silvagni et al., 2016], [Kurdi et al., 2016], [Baker et al., 2016], [Bejiga et al., 2017].

UAV Configurations

UAVs can be classified into several categories depending on their characteristics, such as range, flight altitude, endurance, and payload. The smallest UAVs are the nano (NAV) with a wingspan of less than 15 cm and an endurance of approximately one hour. The largest UAVs are the ones classified in the category of high altitude-long endurance (HALE), which have an endurance of 10-48 hours and a payload of 4,500-15,000 kg [Blyenburgh, 2010-2011]. The miniature UAVs considered to be used in this thesis are typically designed to operate on the order of 10-12 h with payloads of approximately 4-7 kg [Beard and McLain, 2012].

The conventional UAV platforms are generally classified into two main categories: fixed-wing (FW) and rotary-wing (RW) aircraft. The major differences between the two categories are associated with the performance capabilities and structural complexity. Fixed-wing UAVs have the advantage of efficient aerodynamics and require less structural complexity. FW aircraft only have to counteract the resistance that is partially induced by the lifting force of the wings, which is 10-25% of the lifting capacity at low speed, depending on the architecture of the aircraft. Rotary-wing UAVs must generate the entire lifting capacity with their engine. The efficient aerodynamics of FW aircraft enables better performance in terms of endurance, range, and speed for a given amount of fuel compared to RW aircraft. When e.g. medical equipment should be delivered to catastrophe environments, fixed-wing UAVs are to prefer as they are able to carry a heavier payload for a given amount of fuel.

However, platforms based on a fixed-wing configuration require horizontal take-off and landing, while rotary-wing UAVs are capable of vertical take-off and landing. Rotary-wing aircraft also provide a higher level of maneuverability as they are able to hover and rotate at a fixed position. Fixed-wing aircraft have a minimum turning radius and a minimum forward speed, and cannot back or stand still during normal maneuvers.

Due to the ability of longer endurance and greater payload, this project focuses on the development of swarm behavior among fixed-wing aircraft. Take-off and landing are outside the scope of this thesis.

Swarm Intelligence

Teams of small, relatively inexpensive UAVs, each equipped with sensing, communication, computation, and control capabilities, can provide distributed sensing. The overarching requirement for large swarm systems is that the implementation of the design is scalable to any number of vehicles and is robust to the failure of a single vehicle.

Using multiple UAVs enables the designer to create agents which are generally cheaper and less complex compared to a single agent. Examples of swarms intelligence in nature include flocks of birds, schools of fish, herds of animals and colonies of ants or bacteria. The evolution of such behavior is due to its inherent advantages, such as increasing the chance of finding food and avoiding predators. By implementing this type of control, the system will achieve desirable behavior by applying relatively simple laws.

Swarm intelligence based techniques can be used in a number of applications. One example is in the U.S. military where swarm techniques are investigated for controlling unmanned vehicles used for defense and for border surveillance. The European Space Agency is developing an orbital swarm for self-assembly and interferometry, and NASA is investigating the use of swarm technology for planetary mapping. Swarm intelligence may also be used in other applications than for unmanned vehicles, where one example is the possibility of controlling nanobots within a body for the purpose of killing cancer tumors, which is discussed in [Lewis and Bekey, 1992].

By using a swarm of UAVs instead of a single aircraft, the time to fully cover a specific area decreases significantly. The algorithm developed in this thesis is scalable, flexible, and robust to individual failures.

Control Architectures

The control architecture for UAV swarms can be either centralized or decentralized. Centralized control is a method in which each agent is guided along its own path, provided by a central control unit. The central control unit can be either a ground station or one of the members of the swarm, often referred to as the *leader*. Centralized control requires higher bandwidth and problems regarding robustness may occur if the central unit crashes or is exposed to communication problems. As the number of UAVs increase, controlling the system in a centralized way becomes unrealistic. Decentralized control methods have been developed to overcome this problem and in this thesis, control, communication, sensing, and computational tasks are handled on a decentralized basis. In a decentralized control architecture, the individual members of the swarm are their own control unit and react to each others' movements. Decentralized control approaches require a high level of autonomy of the system and the communication between each individual UAV. An individual UAV failure in a decentralized control system will generally not affect the group performance. The benefits of decentralized approaches allow the UAVs to adapt to dynamic environments as the overall behavior of the system is constructed on local collaborations between the agents.

1.2 Previous Work

In recent years, there has been a proliferation of research efforts to study many aspects of cooperatively controlling autonomous multi-agent systems. This thesis tends to fall into a broad range of categories, including UAV aerodynamics, decentralized swarm control design, WPAN networks, radio signal propagation, sensor fusion, and RSSI based position estimation.

Most of the existing work related to swarm intelligence is derived from the social behavior of animals or insects. For swarms of aircraft, most research make use of GPS signals for providing position information. However, there are numerous studies where positions are estimated by measuring the signal strength from access points (APs) with known stationary positions. In this thesis, no APs are positioned on the ground. Instead, the UAVs estimate their position by measuring the signal strength from other UAVs, i.e. all transmitter positions are unknown and dynamic.

In [Yanmas et al., 2011], Wi-Fi signals are used to communicate with an access point on the ground. In [Luo et al., 2013], UAVs communicate through RF signals and RSS values are measured from APs with known positions. The UAVs all have predefined trajectories which are modified if a collision is predicted. All UAVs have different priorities and the UAV with the lowest priority will modify its trajectory to prevent the collision.

Path planning is a common approach for swarms of unmanned aircraft and may be optimal if the search area is known a priori. However, in this thesis, the environment is unknown and no predefined trajectories are applied. Instead, the UAVs are controlled by potential fields computed in real time. Potential fields used to achieve swarm behavior has previously been presented in a numerous of research papers [Hexmoor et al., 2005], [Bandala et al., 2014], [Ge and Cui, 2000]. The latter presents a new potential field method for motion planning of mobile robots in a dynamic environment.

A vast majority of swarm research use UAV networks consisting of homogeneous quad-rotors. Quad-rotors are generally smaller in size and keep shorter distances to each other than fixed-wing aircraft. Most simulations of fixed-wing swarms maintain a constant speed and it is commonly assumed only a single obstacle is detected by a UAV at each time instant. In this thesis, the speed of the UAVs is not constant and multiple obstacles may be detected at a certain time instant.

In most previous research, the UAVs steer towards the center of the swarm. Note that the center of the swarm is unknown when the UAVs are unable to directly communicate with all members of the swarm, due to communication constraints. In the simulations of this thesis, the members interact with neighboring UAVs only. The agents broadcast their position, but the receiver sensitivity limits the distance at which the signals can be detected.

In [Gaudiano et al., 2003], a UAV swarm is used to track targets and different coverage strategies are analyzed. The swarm consists of a maximum of 10 UAVs with known positions. The environment is subdivided into a grid map and the UAVs turn automatically as they approach the border of the area of interest. No obstacles are present, and there is no risk of colliding with targets as they are positioned on the ground.

A simulation of a UAV swarm is presented in [Yokoyama et al., 2014], where a malicious UAV provides false positions to deceive other members of the swarm. By obtaining access to the network, the UAV successfully attacks other agents. The swarm consists of 5 quadcopters, and a multilateration verifier technique is conducted from RSSI measurements. For the RSSI simulation, the effect of antenna characteristics, antenna orientation, and signal propagation disturbances are not taken into account. Instead, the study focuses on security within wireless networks.

Details on previous work on certain topics are further described in the corresponding sections.

1.3 Goal and Approach

The goal of this thesis is to develop, implement, and evaluate algorithms for outdoor positioning and swarm behavior. The swarm should be able to handle individual failures and obtain different high-level tasks. In order to achieve desirable swarm behavior, the swarm is controlled by the use of repulsive and attractive potentials. In the development of this approach, the UAV positions are first assumed to be accurately provided, and thereafter, the positions are estimated from received signal strength measurements. First, the position estimation is performed using information from RSSI combined by a weighted nonlinear least square filter (WNLS). Further, the goal is to improve the performance by adding information from the dynamic motion model and a Kalman filter in order to receive a more accurate model of the UAVs' movements. The results from the two simulations are compared and the possibility to achieve satisfactory behavior with RSSI based position estimation is further analyzed.

1.4 Delimitation and Assumptions

The UAVs are simulated to fly at a constant altitude, which narrows down the positioning problem to a 2-D environment. All members of the swarm are located at the same altitude at all times. The developed positioning approach requires at least three transmitter positions to be provided, either known or estimated. The initial positions of the UAVs need to be known without using GPS signals. These positions may be computed through a minimum of three access points on the ground with known positions. Another way of solving this is to let the UAVs operate in a local coordinate frame and ignore their global position. A third way to account for this is to assume the UAVs know their initial position as long as both their starting position on the ground and their take-off flight path are known.

The UAVs are assumed to be equipped with various sensors, such as gyroscopes, accelerometers, and compasses. Surveillance sensors are used to detect potential victims on the ground and each UAV is assumed to be equipped with a single, downward pointing camera. The camera is assumed to always point straight down, i.e. either both the pitch and roll angles of the aircraft are always zero, or the camera is jointly connected in its center of mass and always points towards gravity. In order to detect targets, either an operator investigates the images in real time, or computer vision algorithms, such as feature tracking, are used to recognize pixels in the images. The grid map of the covered regions is shared between agents and updated in real time with no time delays. Available sensors shall also include distance sensors, e.g. laser/radar/lidar/ladar, used to detect obstacles. Another valid simplification is assuming a flat Earth model.

No weather conditions are taken into account for these simulations, e.g. disturbances like wind, rain, or clouds that can obscure the view of the surveillance sensor are all neglected.

The Kalman filter is optimal in the sense that it minimizes the mean square error of the estimated parameters when Gaussian noise is assumed. In order to use a KF, the noise is estimated as Gaussian for simplicity. Only the mean and standard deviation of the noise are provided, so if the noise is non-Gaussian, the KF may not attain accurate estimates.

1.5 Challenges

In search and rescue operations, it is of great importance to properly analyze the quality and trustworthiness of the reported information. The probability of false negative should remain low, i.e. victims should not go undetected when a UAV is surveying an area. At the same time, to avoid sending a ground rescue team to a place of no interest, a victim should not be falsely detected when it is not present, i.e. the probability of false positive should also remain low. The challenge is to establish accurate models of the quality of the sensory data obtained from the UAVs.

When multiple UAVs are deployed, the sensory data they collect can be shared to generate a complete picture of the environment, which can in turn guide the search process. This task is challenging as it needs to account for limitations in terms of processing, memory storage, energy consumption, network availability, etc. How frequently the connections between UAVs should be established as well as how frequently the UAVs report to a ground station are both important aspects that need to be determined.

When designing the potential field algorithm, many factors are taken into account. The UAVs should maintain a certain distance to their closest neighbor such that the entire area between them is covered and at the same time, no collisions occur and the distance does not exceed maximum communication range. Another important requirement is that the individual flight paths should not be oscillating. The parameters of the potential functions are tuned to achieve desirable results.

Furthermore, for the RSSI measurements, sufficiently good models of the path loss are needed. This, in turn, requires information about the power with which the communication modules transmit and how dense the environment is. Signal disturbances may distort the signal significantly. If there is an obstacle obstructing the signal path, the RSSI will decrease and the position estimate will be affected. The model of the position estimation has to take account for this. Antenna characteristics and the effect of antenna localization need to be studied thoroughly.

For real search and rescue operations with small UAVs, weather conditions need to be taken into account. However, as mentioned in the previous section, this aspect is outside the scope of the thesis.

1.6 Platform

In this project, two Genuino UNO microcontrollers are used in combination with two XBee S1 PRO communication modules and two XBee shields. These devices are used to send and receive data packages between two nodes. One communication module measures the received signal strength from incoming packages and estimates the distance to the other. A servo motor is attached to the transmitter in order to see how the signal strength is affected by the angle of transmission.

Genuino UNO

An Arduino/Genuino UNO is a microcontroller board which can communicate with servo motors and a multitude of different sensors via analog input pins and digital input/output pins. The microcontroller can be connected to a computer with a USB cable or powered by either a battery or an AC/DC adapter. Programs are written in the Arduino Integrated Development Environment (IDE) and thereafter uploaded to the microcontroller.

Since 2005, when the Arduino project was initiated, all their products are distributed as open-source hardware and software. In May 2015, Arduino LLC created the worldwide trademark *Genuino*, used as the brand name outside the United States.

XBee

XBee modules are embedded solutions providing wireless end-point connectivity to devices. The IEEE 802.15.4 networking protocol is used for fast point-to-multipoint or peer-to-peer networking. XBee is a Zigbee based protocol, where ZigBee is a wireless 2.4 GHz standard built on IEEE 802.15.4. ZigBee is a mesh network and each node in a ZigBee system can act as either a wireless data endpoint or a repeater.

These modules are designed for high-throughput applications requiring low latency and predictable communication timing. In order to configure the XBees and set their baud rate, they are individually connected to a PC with an XBee explorer before mounted on the Genuino via an XBee shield.

Application Programming Interface (API) mode is a frame-based method for sending and receiving data to and from a radio's serial UART. The API mode allows the programmer the ability to view RSSI and source addresses on a packet-by-packet basis and receive packet delivery confirmation on every transmitted packet. By having the XBees configured in API mode it is possible to communicate through a Genuino. The communication modules used in this thesis are the XBee S1 PRO which has a receiver sensitivity of -110 dBm. The measurement data collection has been performed using the software programs Arduino IDE and MATLAB.

1.7 Outline

This section briefly presents the structure of the thesis.

Chapter 2 gives a brief background on navigation techniques and common onboard sensors for UAVs. In Chapter 3, general swarm behavior is introduced, both natural and artificial. Chapter 4 presents artificial potential fields applied to swarm intelligence. An introduction to WPAN and wireless sensor networks is provided in Chapter 5. Radio propagation patterns, antenna characteristics, and radio signal disturbances are described in Chapter 6. Chapter 7 further explains how RSSI signals may be used for positioning applications and introduces the theory behind sensor fusion. In Chapter 8, aerodynamics and 2-D kinematics of fixed-wing UAVs are discussed. Chapter 9 presents different non-linear filtering techniques, introducing some filters applied in this thesis. Chapter 10 is dedicated to the parameter evaluations of the RSSI-distance models discussed in Chapter 7. In this chapter, the experimental setup for the RSSI measurements is presented. Chapter 11 provides detailed information on the MATLAB simulations, for both UAVs with known and estimated positions. Chapter 12 thoroughly evaluates the results of the thesis, including the evaluation of the RSSI-distance model and several simulation results. Lastly, in Chapter 13, the conclusions of the thesis is discussed and possible future work on the subject is presented.

2

Background on Navigation

In this chapter, a brief introduction to navigation techniques is given. Firstly, the concept of GPS is explained and secondly, rotation matrices and different coordinate systems are presented. Further, typical onboard sensors for UAVs are presented, including accelerometers, gyroscopes, pressure sensors, and magnetometers.

2.1 GPS

The GPS system was launched in the United States in 1973, consisting of 24 satellites orbiting the Earth at an altitude of approximately 20200 km. The system was developed by the U.S. Department of Defense and became fully operational in 1993 [Mai, 2012]. In order to estimate a position on the Earth's surface, it requires to be seen by at least four satellites at all times. Each satellite broadcasts radio signals with their own position, a pseudo-random code known to the receiver and the time of transmission (TOT). The GPS signal travels at the speed of light and the receiver measures the time of arrival (TOA) of at least four satellite signals. From the TOAs and TOTs, the receiver forms time of flight (TOF) values which gives an estimate of the distance to the satellites. By applying these TOFs to a multilateration algorithm, the receiver estimates its latitude, longitude, altitude, and clock-time offset. A simple GPS system is illustrated in Figure 2.1.

The GPS system provides a position accuracy of approximately five meters for points in unobstructed line-of-sight (LOS) [Trimble, 2017]. If the satellites are not in LOS from the GPS receiver, problems with positioning accuracy might occur. Putting more satellites in orbit increases the probability of having enough satellites visible at the entire surface of the Earth. In urban environments or indoors, the signal path may either be obstructed by buildings in the receiver's surroundings, or by the building the receiver is located in, respectively. These obstructions may result in signal reflection, diffraction, and scattering. Since the distance is estimated from the time it takes for the signal to travel from the satellite to the receiver, these signal disturbances lead to an increase in the distance estimate. An obstruction may even make the signal too weak for the receiver to detect [Grimes, 2008].

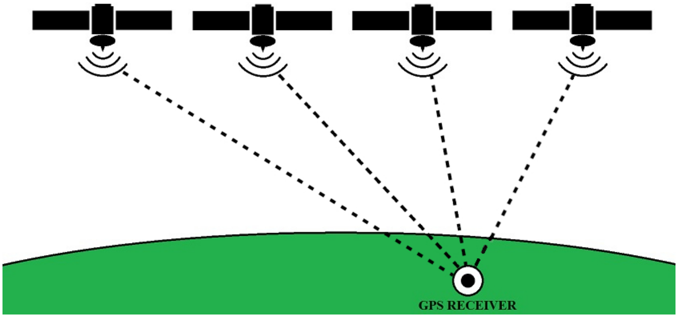

Figure 2.1 Illustration of a GPS system.

There is a multitude of alternative techniques for positioning estimation applications. These techniques include using magnetic fields, cameras, signal strength communication, inertial sensors, etc. [Mautz, 2012].

2.2 Coordinate Systems

When studying unmanned aircraft systems, it is important to understand how different bodies are oriented relative to each other. To understand how the aircraft is oriented with respect to the Earth is essential for these studies. Other important aspects are knowledge of how a camera or sensor is oriented relative to the aircraft and how an antenna is oriented relative to a signal source on the ground or to another aircraft. It is necessary to use different coordinate systems for the following reasons [Atkins et al., 2016]:

- The motion of an aircraft is most easily described in a body-fixed reference frame, while Newton's equations of motion are derived relative to a fixed, inertial reference frame.
- Onboard sensors, such as accelerometers and gyroscopes, measure information with respect to the body-fixed frame. If the aircraft is equipped with a GPS, it measures position, ground speed V_g, and coarse angle χ, with respect to the inertial frame.
- A majority of mission requirements, such as map information, flight trajectories, and loiter points, are specified in the inertial frame.

A well-defined coordinate system is of great importance for position applications. One coordinate frame can be transformed into another through two basic operations: rotation and translation. Throughout this thesis, a flat, non-rotating earth is a valid assumption.

Rotation Matrices

Let a coordinate be denoted as $\mathbf{x}$ in the inertial frame and as $\mathbf{x}_b$ in the body frame of reference. The body frame has a different angular orientation, but for now, it is assumed their origins are coincident. There are multiple ways of describing angular orientation, including Euler angles and Euler parameters (quaternions). These representations are further described in Chapter 8. This section demonstrates an example of how to represent a coordinate in inertial space, referenced to a rotated body frame. The transformation takes the form of a 3x3 matrix, which is derived through successive rotations of the three Euler angles. Figure 2.2 illustrates the transformation of a coordinate frame to an arbitrary orientation.

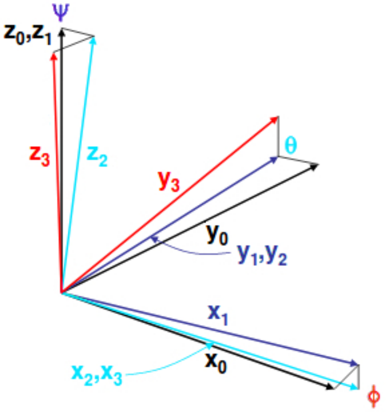

Figure 2.2 Transformation of a coordinate frame by rotations of the three Euler angles.

Before the first rotation takes place, the point's coordinates in the inertial frame equals the body-referenced coordinates, $\mathbf{x} = \mathbf{x}_b^0$. First, the z axis of the body-fixed frame is rotated through the yaw angle ψ.

$$\mathbf{x}_b^1 = \begin{bmatrix} \cos\psi & \sin\psi & 0 \\ -\sin\psi & \cos\psi & 0 \\ 0 & 0 & 1 \end{bmatrix} \mathbf{x}_b^0 = R(\psi)\mathbf{x}_b^0 \tag{2.1}$$

The x and y axes are modified according to rules of basic trigonometry, while the rotation about the z axis does not change the point's z coordinate. The second rotation is applied about the new y axis through the pitch angle θ.

$$\mathbf{x}_b^2 = \begin{bmatrix} \cos\theta & 0 & -\sin\theta \\ 0 & 1 & 0 \\ \sin\theta & 0 & \cos\theta \end{bmatrix} \mathbf{x}_b^1 = R(\theta)\mathbf{x}_b^1 \tag{2.2}$$

The final rotation is about the new x axis through the roll angle ϕ.

$$\mathbf{x}_b^3 = \begin{bmatrix} 1 & 0 & 0 \\ 0 & \cos\phi & \sin\phi \\ 0 & -\sin\phi & \cos\phi \end{bmatrix} \mathbf{x}_b^2 = R(\phi)\mathbf{x}_b^2 \tag{2.3}$$

Further on, the notation $\mathbf{x}_b^3$ is replaced by $\mathbf{x}_b$. The three rotations can be cascaded through matrix multiplication, see (2.4), where c is short for *cosine* and s for *sine*. Note that the rotation matrices are noncommutative, i.e. the order of the rotations matters.

$$\begin{aligned} \mathbf{x}_b &= R(\phi)R(\theta)R(\psi)\mathbf{x} \\ &= \begin{bmatrix} c\theta c\psi & c\theta s\psi & -s\theta \\ -c\phi s\psi + s\phi s\theta c\psi & c\phi c\psi + s\phi s\theta s\psi & s\phi c\theta \\ s\phi s\psi + c\phi s\theta c\psi & -s\phi c\psi + c\phi s\theta c\psi & c\phi c\theta \end{bmatrix} \mathbf{x} \\ &= R(\psi, \theta, \phi)\mathbf{x} \end{aligned} \tag{2.4}$$

Rotation matrices are orthonormal, i.e. $\mathbf{x} = R^T\mathbf{x}_b$. Note that throughout this section, the origins were assumed to coincide. If the body frame has a different origin than the inertial frame, the offset is added to the equation as $\mathbf{x} = \mathbf{x}_0 + R^T\mathbf{x}_b$. The most important coordinate systems for UAVs are described below and illustrated in Figure 2.3.

Inertial Frame

The inertial coordinate system is an Earth-fixed coordinate system with its origin at a defined home location. For inertial coordinate systems, Newton's laws of motion hold true. As mentioned previously, the Earth is assumed to be non-rotating with a flat xy-plane and therefore, the Earth frame is approximated as inertial. The coordinate system is sometimes referred to as the *NED* reference frame, where x is positive in the direction of north, y is positive in the direction of east and z is positive towards the center of the Earth.

Vehicle Frame

The vehicle frame is aligned with the inertial frame but has a different origin. When studying unmanned aircraft, the origin is at the center of gravity of the UAV. All three coordinate frames presented below have their origin at the aircraft's center of gravity.

Body Frame

The x axis of the body frame is out the nose of the aircraft, positive in the direction of flight. The y axis is positive out the right wing and the z axis is perpendicular to the x axis, positive below the aircraft. In this thesis, the aircraft are assumed to be symmetric from right-to-left and the z axis is therefore in the plane of symmetry.

Wind Frame

Aerodynamic forces and moments acting on an aircraft are usually expressed in the wind frame. The wind frame has its x axis positive along the velocity vector of the aircraft relative to the air, i.e. the z axis is rotated by the sideslip angle β from the stability frame. The sideslip angle is the angle between the velocity vector and the projection of the aircraft's longitudinal axis on the xy-plane in the wind frame.

Stability Frame

The stability frame is rotated by the angle of attack α among the y axis, such that the velocity vector is in the xy-plane. The angle of attack is the angle between the xy-plane in the wind frame and the aircraft's longitudinal axis.

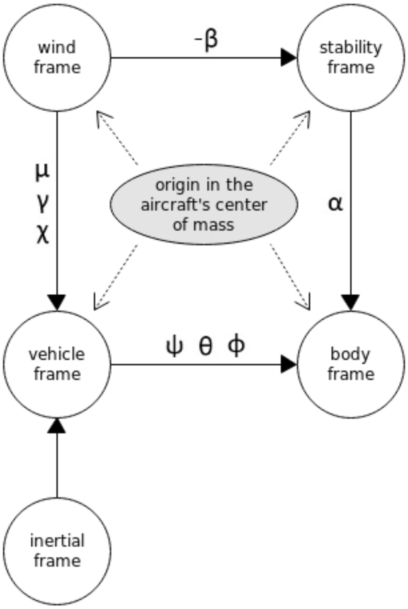

Figure 2.3 Different coordinate systems referred to in this thesis. β is the sideslip angle and α is the angle of attack. ψ, θ, and ϕ are the yaw, pitch, and roll angles. χ, μ, and γ are the heading, bank, and flight path angles and analogous to ψ, θ, and ϕ respectively. The inertial frame and the vehicle frame are differentiated by a parallel dislocation.

2.3 Sensors

The objective of this section is to describe the onboard sensors a UAV is typically equipped with and further quantify what they measure. Sensors used for guidance, navigation, and control are in focus, whilst payload sensors, e.g. cameras, are not described in detail. By combining the measurements from multiple sensors the autopilot can keep an aircraft stable very effectively. Most flight controllers have 6 degrees of freedom (DOF), which means they have a 3-axis accelerometer and a 3-axis gyroscope.

Accelerometer

An accelerometer is an electromechanical device which is used to measure both static and dynamic acceleration forces along one or multiple axes. The force of gravity is an example of a static force, while movement or vibration in mobile devices are examples of dynamic forces. Conceptually, an accelerometer behaves like a damped mass on a spring. A proof mass is displaced when the accelerometer is exposed to acceleration and the spring accelerates the mass at the same rate as the casing. The acceleration is found by measuring the displacement of the mass, i.e. the displacement by the spring in the suspension. A simple force balance analysis of the proof mass yields the following relationship

$$m\ddot{x} + kx + ky(t) \tag{2.5}$$

where x is the inertial position of the proof mass and $y(t)$ is the inertial position of the housing. The deflection of the suspension can be expressed as $\delta = y(t) - x$ and Equation (2.5) is rewritten as

$$\ddot{x} = \frac{k}{m}\delta \tag{2.6}$$

which shows that the acceleration of the proof mass is proportional to the deflection of the suspension. At frequencies below the resonant frequency, the acceleration of the proof mass is the same as the acceleration of the housing. For further details see [Beard and McLain, 2012]. Accelerometers are commonly mounted near the aircraft's center of mass with the sensitive axis of one accelerometer aligned with each of the body axes. The vectors $\mathbf{a}_m$ reported by the accelerometer represent the total acceleration of the casing subtracted by the gravity.

$$\mathbf{a}_m = \mathbf{a}_b - \mathbf{R}_v^b \begin{pmatrix} 0 \\ 0 \\ g \end{pmatrix} \tag{2.7}$$

In (2.7), g represents the acceleration of gravity and $\mathbf{a}_b$ is the total acceleration of the casing seen in the body frame. $\mathbf{R}_v^b$ is the rotation matrix from the vehicle frame to the body frame. This model assumes that there is no cross-axis alignment, scale factor, or bias errors in the measurements. The accelerometer measurements are dependent on its placement on the aircraft. If there is an offset between the sensor's position and the center of gravity of the aircraft, the measurement needs to be transformed. The transformation make use of the distance to the new point and the aircraft's angular velocity and angular acceleration.

Gyroscope

Gyroscopes are essential for measuring or maintaining orientation. A typical airplane uses gyroscopes in everything from its autopilot to its compass. A three DOF gyro measures the angular velocity with which it is turning around the pitch, roll, and yaw axis. Mechanically gyros consist of a spinning wheel or a disc mounted on a gimbal, which allows the wheel to rotate freely about each axis. Once a gyroscope spins, its axes want to keep pointing in the same direction and according to the conservation of angular momentum, the orientation of the axis of rotation is unaffected by tilting or rotation of the mounting.

Unlike a magnetic compass, a gyroscope only measures how the angles change over time and does not seek north. When a gyroscope is mounted on an aircraft, it will drift over time and needs to be recalibrated periodically, using a magnetic compass as a reference.

A rotating disc is not a well-suited gyroscope for small UAVs. Instead, MEMS gyroscopes are used in these applications. MEMS rate gyros typically consist of a proof mass on a cantilever actuated at their resonant frequency to cause oscillation in the vertical plane. The cantilever is actuated such that the velocity caused by the oscillations has constant amplitude, see (2.8).

$$\mathbf{v} = A\omega_n \sin(\omega_n t) \tag{2.8}$$

In (2.8), A is the amplitude of the oscillation and ω_n is the natural frequency. If the sensitive axis of the gyro is configured to be the longitudinal axis of the undeflected cantilever, then the rotation about the axis will result in a *Coriolis acceleration* in the horizontal plane described by (2.9).

$$\mathbf{a}_C = 2\Omega \times \mathbf{v} \tag{2.9}$$

$\Omega = (\dot{\theta}, \dot{\phi}, \dot{\psi})$ are the angular velocities of the body in an inertial reference frame, and $\mathbf{v}$ is the velocity of the point in the reference frame of the body. The French scientist C.G de Coriolis discovered in the early 19th century that a point translating on a rotating rigid body experiences an acceleration that is proportional to the velocity of the point and the rate of rotation of the body [Beard and McLain, 2012]. The Coriolis acceleration of the proof mass results in a lateral deflection of the cantilever, which can be detected by a multitude of techniques. This can be compared to the behavior of the proof mass and the cantilever of the accelerometer.

Pressure sensor

Pressure is defined as the force per unit area acting on a surface and acts in the direction normal to the surface of the body to which it is applied. For UAVs, pressure measurements provide indications of both the altitude and the airspeed of the aircraft. For these measurements, an absolute pressure sensor and a differential pressure sensor are used, respectively. For further details, the interested reader is referred to [Beard and McLain, 2012].

Magnetometer

The magnetic field of the Earth has been used for navigational applications for centuries and is still useful when navigating a variety of vehicles, including unmanned aircraft. The Earth's magnetic field behaves similarly to a magnetic dipole with magnetic field lines running normal to the surface of the Earth at the poles and parallel to the Earth's surface near the equator. Compasses provide an indication of the heading relative to the magnetic north ψ_m by measuring the direction of the magnetic field locally. The heading angle ψ is the sum of the magnetic declination angle δ and the magnetic heading measurement.

$$\psi = \delta + \psi_m \tag{2.10}$$

The declination angle is the angle between true north and magnetic north. For any given latitude and longitude, δ can be calculated using a multitude of different models. The magnetic heading can be determined from measurements of body-frame components of the magnetic field strength projected onto the horizontal plane. For further reading, see [Beard and McLain, 2012].

Magnetometers and digital compasses can be sensitive to electromagnetic interference. When the sensor is mounted on a UAV, it is essential to avoid interference from electrical motors, servos, and power wiring. Metallic objects in general may also disturb the magnetometer.

3

Background on Swarm Behavior

Swarm intelligence refers to the collective behavior of self-organized systems that can consist of both natural and artificial agents. The terminology was first introduced by Jing Wang and Gerardo Beni in 1989, in the context of robotic systems [Beni and Wang, 1989]. In nature, when organisms travel in groups, they exhibit certain behaviors. This phenomenon occurs at both microscopic and macroscopic scales and examples of swarm intelligence in nature include colonies of ants, flocks of birds, herds of animals, schools of fish, and growth of bacteria [Partridge, 1982]. This behavior can be simulated in computers programs combining sets of different rules.

The first simulation of flocking behavior was created in 1987 in a computer program called Boids, developed by Craig Reynolds [Reynolds, 1987]. This program simulates simple agents (boids) allowing them to move individually according to three basic rules.

- Separation - steer to avoid collisions with nearby flockmates.
- Alignment - steer towards the average heading of nearby flockmates.
- Cohesion - steer to move towards the average position of nearby flockmates.

Each boid has direct access to the whole area it is operating in, but to attain flocking behavior, a boid should only interact with flockmates within a limited area around itself. This neighborhood is characterized by a distance and an angle measured from the center of the boid and the boid's heading angle, respectively. This behavior can be compared to the general behavior of school's of fish, where the focal fish pays attention to all fish within a small zone of repulsion, a zone of alignment, and a larger zone of attraction [Couzin et al., 2002]. The model can be extended with more complex rules, such as obstacle avoidance and goal seeking.

A swarm typically consists of simple agents interacting locally with one another and their environment. Swarm members are naturally disorganized and perform very simple tasks in response to environmental information as well as local information from other group members. Even without a centralized control structure, local interactions between agents lead to the emerge of intelligent global behaviors. The agents are unaware of what problem they are collectively working on, but based on local communication with nearby members and the actions that they exhibit, an individual evaluates an appropriate behavior that will contribute to the swarm's objective.

Some biological swarms fly in formations, i.e. follow a geometric configuration. Flight formation can be used in order to conserve the energy and effort each individual exert. Flocks of birds use formation to easier catch pray and to avoid predators [Deneubourg and Goss, 1989].

This chapter further explains robotic swarms and discusses different models of swarm behavior.

3.1 Robotic Swarms

Agents in robotic swarms are programmed to perform simple tasks based on a set of rules. In decentralized control systems, robots communicate directly without any base station support. Different techniques can be used for decentralized communication, such as WiFi, Bluetooth, or ZigBee.

For swarms of unmanned aerial vehicles, agents generally evaluate different potential paths against the following high-level objectives [Sauter et al., 2009]:

- Prefer to move in a straight line to conserve fuel.
- Prefer to move at optimal airspeed to conserve energy.
- Prefer to fly at a constant altitude to conserve energy.
- Stay away from neighboring agents to avoid collisions.
- Stay within communication range to other agents in order to maintain a fully connected network.
- Stay away from no-go zones, such as obstacles or enemies.

Compared to most swarm behavior found in nature, robotic swarms can be simulated without blind angles, i.e. the agents are equipped with sensors with an all-round coverage.

UAV Control Strategies

There are several control strategies for UAV swarms, where the decision making is based either on the information available in the immediate surroundings of each UAV, or the information from the entire search area. Four different strategies of decentralized control are listed below and evaluated in [Gaudiano et al., 2003].

- The *baseline strategy* is the simplest decentralized control method. The UAVs fly in a straight line until they reach the boundary of the search area and thereafter make a turn.

- The *random strategy* is a slightly altered version of the baseline strategy and allows the UAVs to change its heading by a small random angle at each time step.

- The *repulsion strategy* is based on potential forces, where each UAV can sense other UAVs within a certain radius. To keep a fully connected network and to prevent collisions, the UAVs maneuver based on the distance to other UAVs.

- In a *pheromone strategy*, the UAVs leave a marker along their flight paths to indicate that a cell has been visited. Other swarm members can sense the pheromone level in their local surroundings and adjust their flight path in order to search for unvisited cells.

3.2 Models of Swarm Behavior

There are multiple ways of simulating swarms, where most of the techniques are based on biological systems. This section presents some previous work on swarm behavior.

Particle Swarm Optimization

Particle swarm optimization (PSO) is a population-based stochastic optimization method developed by Kennedy, Shi, and Eberhart [Kennedy, 1995], [Shi and Eberhart, 1998]. PSO algorithms optimize a problem by iteratively trying to improve a solution with regard to a given measure of quality. The optimal solution can be represented as a point or surface in an n-dimensional space. Particles move around in the solution space according to simple mathematical formulas. Each particle keep their previous best position in memory and their movement is based on this position and the best known position of the swarm. After each time step, the particles are evaluated according to some fitness criterion. Over time, particles accelerate towards the particles within their communication range with better fitness values. The large number of members that the particle swarm consists of makes this method impressively resilient to the problem of local minima, which gives this approach a major advantage over other global minimization strategies [Ruan, 2010].

Pigeon-inspired Optimization

Pigeon-inspired optimization (PIO) is a swarm intelligence algorithm inspired by the homing behavior of pigeons. In PIO simulations, the two following operators are designed to imitate the homing characteristics of pigeons:

- Map and compass operator: pigeons use magnetoreception to create a map of the Earth's magnetic field. They adjust their direction of flight by referring to the altitude of the sun as a compass.
- Landmark operator: when pigeons fly close to their destination, they rely on nearby landmarks. If the pigeons recognize the landmarks, they fly straight to the destination. If they are far from the destination and unfamiliar to the landmarks, they follow the pigeons who are familiar with the landmarks.

This is a path planning algorithm which requires danger regions to be known, see details in [Duan and Qiao, 2014].

Potential Fields

Potential fields used in swarming applications was first proposed by Khatib in 1985 [Khatib, 1985]. Swarm members treat the goal position as an attractive potential, while threats, such as obstacles or enemies, are represented by repulsive potentials. Unexplored areas of the terrain can also be treated as attractive potentials. Potential fields could be combined with rapidly exploring random trees (RRT) which generate a tree of trajectories by randomly selecting a point in the given space. Each branch is tested for collision avoidance before adding it to the tree until a connectivity is formed between the start and goal position [Beard and McLain, 2012]. A potential field algorithm is developed in this thesis and further described in Chapter 4.

Ant Colony Optimization

The use of pheromones is a key concept in insect-inspired swarm control. Ants deposit pheromones in order to inform their nestmates where food has been found. When an ant leaves the nest it explores randomly until it finds a pheromone trail or until it finds food. When an ant has found food it follows the pheromone trail back to the nest and repeats the procedure. Ants also deposit small amounts of repulsive pheromones when they have thoroughly explored an area without any luck of finding food [Stickland et al., 1999].

Pheromones can be considered as guidelines to tell agents whether an area is attractive or unattractive for future exploration. This algorithm allows swarm members to use local pheromone levels to determine which direction they should go. Each member of the swarm can change simple parameters relating to pheromones to influence the movement of the swarm.

Digital pheromones are used in computer algorithms to control the movements of individual agents and steer them toward areas that are attractive, and away from areas that are dangerous or unattractive. Areas that are already explored are commonly characterized by repulsive pheromones. For digital pheromone-based algorithms, pheromone levels are shared between agents over communication networks. The area of interest is discretized into a grid, where the cells contain all pheromone flavors present. There are generally five different flavors, where each sensor maintains its own version of a pheromone map. Unsearched areas contain attractive pheromone levels. When a sensor has detected a possible target but an additional sensor is required to identify it, a sensor request pheromone is deposited. In [Sauter et al., 2009], there is also a target tracking pheromone, a no-go pheromone, and a path pheromone deposited along the planned path for each swarm member.

For this control to be effective, the commander needs a clear understanding of the entire area of interest and what the swarm members should focus on. A fundamental challenge with pheromone-based algorithms is that they are computationally expensive for large fields.

In this thesis, the search area is discretized into a grid, where unexplored cells contain an attractive pheromone. If a cell is scanned and no victim is detected, the cell is neutralized.

3.3 Waypoint Guidance

There are other ways of controlling swarms, where waypoint guidance is a common technique when the search area is known. Waypoint guidance is a path planning technique, where the Dubins path is one of the most common used algorithms for 2-D environments. A Dubins path is a minimum time trajectory between two points consisting of straight lines and circular arcs of maximum curvature. In order to get from one point to another in the same plane, the control parameter changes maximum twice, see Figure 3.1 for examples.

In Figure 3.1, S represents a straight line, R a right turn, and L a left turn. Note that this is a 2-D environment, i.e. the aircraft maintains a constant altitude.

Extensions of Dubins paths have been developed to satisfy curvature constraints in 3-D environments. An algorithm for tracking a 3-D Dubins path was presented in [Ambrosino et al., 2009].

Path planning algorithms are generally based on the knowledge of the environment. In this thesis, the presence of trees and other obstacles are unknown a priori, and exceptions of the control algorithm have to be made in real time when obstacles are detected. To keep the control loop simple and generic, no special cases are allowed and path planning is not used in this study.

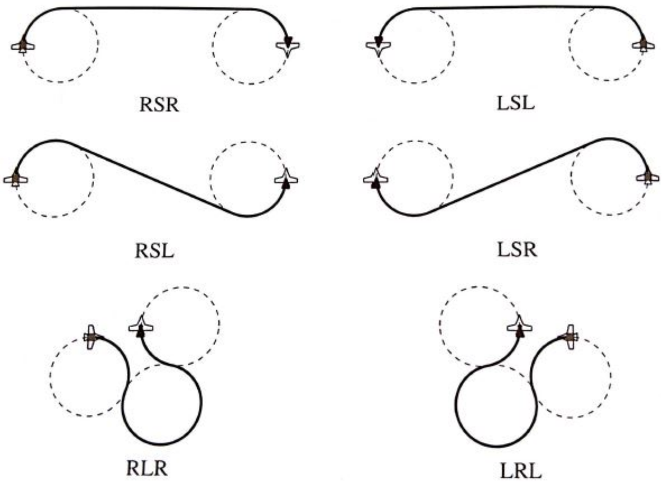

Figure 3.1 Example of Dubins paths connecting pairs of configurations in the plane. (Reprinted with permission from [Atkins et al., 2016]. ©John Wiley and Sons.)

4

Artificial Potential Fields

Artificial potential fields are an example of a behavioral control architecture and were first introduced in [Khatib, 1985]. The basic idea is to create a workspace where each member of the swarm is attracted towards a goal state with a repulsive potential ensuring collision avoidance [Ge and Cui, 2000]. Artificial potential functions can be implemented to construct attractive-repulsive relations among swarm members. The design procedure is based on potential functions which are chosen such that the corresponding potential field is attractive for agent pairs with large inter-agent distances and repulsive for short inter-agent distances, i.e. the attractive part dominates on large distances and the repulsive part dominates on short distances. The attractive potential function results in aggregation and the repulsive function results in collision avoidance between agents [Gazi et al., 2007]. In this chapter, the potential functions implemented in the MATLAB simulations are further explained.

4.1 Potential Fields in MATLAB Simulations

Potential functions for inter-agent interactions are essential for potential field based swarm control. When implementing the desired swarm behavior of this thesis, additional potential functions are required. The area of interest is decomposed into a set of grid cells, where an attractive potential is centered in each unscanned cell in order to steer the swarm towards unexplored areas. Multiple static obstacles with repulsive potentials are randomly deployed in the search area. The general characteristics of these four potential functions are illustrated in Figure 4.1. Note that the values on the x axis are not numerically specified since these depend on the sensors and communication modules used. The potentials are scaled down and obtain values from 0 to 1, and each agent can sense multiple agents simultaneously.

In Figure 4.1, U_{rep} and U_{atr} represent the inter-agent potentials when the UAVs have equal heading angles. These potentials are both functions of the distance between agent pairs. U_{obs} and U_{cell} represent the repulsive potential from obstacles and the attractive potential to unvisited cells when they are in line with the heading angle. These potentials are functions of distance from the agent to an obstacle and from an agent to a cell, respectively.

The potentials are also affected by the difference in yaw, the angles to obstacles, and the angles to cells. How these angles affect the different potentials is further described in the upcoming subsection.

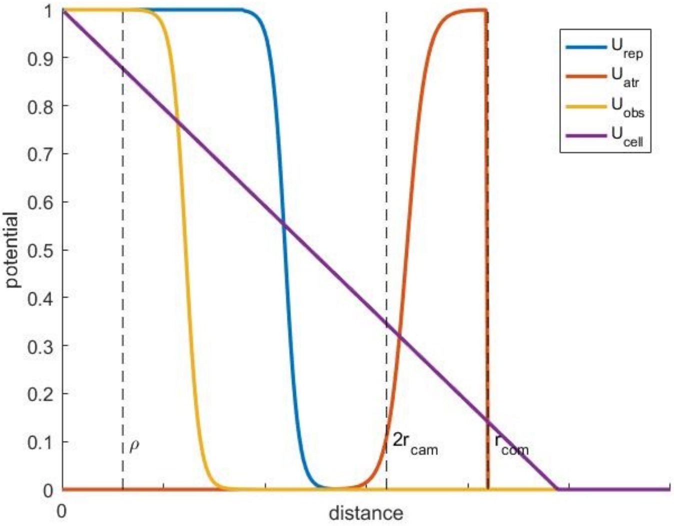

Figure 4.1 Attractive and repulsive potentials from agents, obstacles, and cells as a function of distance. ρ is the minimum turning radius of the aircraft, the radius of the surveillance camera is denoted as r_{cam}, and r_{com} represents the maximum communication range.

The inter-agent repulsive and attractive potentials in Figure 4.1 are opposed and when the distance between an agent pair is within a certain distance interval the agents will not be exposed to any potential forces. For an optimal solution, the distance between agents should be twice the surveillance camera radius (r_{cam}) for the entire area between an agent pair to be covered. To eliminate the risk of missed areas, the desired distance between agents is chosen such that there is a small camera overlap, which results in a distance marginally smaller than $2r_{cam}$.

The red line in Figure 4.1 represents the attractive potential between agents, which is zero when the UAVs are out of communication range. The blue curve illustrates the repulsive potential between agents, which decreases with increased distance and reaches zero as the distance approaches $2r_{cam}$.

The yellow curve in Figure 4.1 represents the repulsive potential from obstacles. In practice, the obstacles are detected by a sensor, such as ultrasonic, infrared, vision, or laser. In this thesis, collisions are avoided by turning either left or right, since the agents are limited to fly at a constant altitude and therefore can not chose to fly above obstacles in order to prevent collisions, see Figure 4.2. The repulsive potential from obstacles is greater for shorter distances and approaches zero when the obstacle cannot be detected by a sensor. To prevent collisions, this potential should reach its maximum when the UAV flies straight towards an obstacle and the distance approaches the minimum turning radius ρ of the UAV. This approach would generally work for moving obstacles with simple dynamics as well.

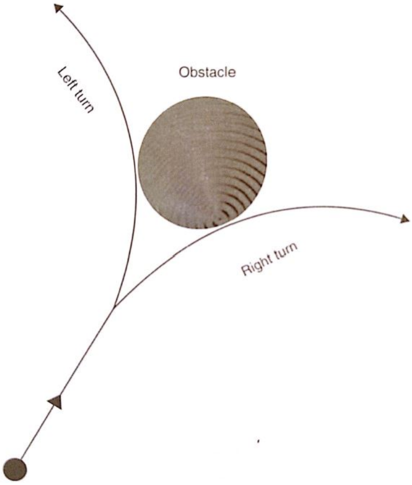

Figure 4.2 Only two possibilities are available for obstacle avoidance for fixed-wing aircraft in 2-D. They can fly either on the left side or on the right side of the obstacle. (Reprinted with permission from [Atkins et al., 2016]. ©John Wiley and Sons.)

However, problems may occur if there is a collection of many obstacles in an area, such as a forest with trees taller than the aircraft's altitude. If the swarm splits up around the group of obstacles, they will most likely loose each other and create two subswarms. If the distance between the two groups is greater than the maximum communication range, they will not know where the other agents are located. After passing an obstacle, the UAVs may broadcast data packages to all agents within their communication range in order to investigate if all agents are still connected. If the number of UAVs connected has decreased after avoiding obstacles, the agents can apply dead reckoning by using the heading angle and position they obtained before they turned to avoid the collision. This type of control is undesirable, as it creates special cases. The control system should be generic and stay simple with communication kept to a minimum. The same problem occurs when there is a single, large obstacle present, e.g. a mountain or a tall building. In the simulations of this thesis, only small static obstacles are used.

The purple line in Figure 4.1 is a linear function of the distance to an unvisited cell and depends on how many cells we take into account when computing the attractive potential. The attraction to cells cannot exceed the repulsive potential from obstacles or the repulsive potential between UAVs since that will result in collisions. If the attraction to cells is much greater than the attraction between agents, chances are the UAVs will take individual paths and loose each other.

Heading Angle Dependencies

If two agents are flying away from each other, the attractive potential between them is proportional to the difference in yaw, while the repulsive potential is inversely proportional. The opposite holds true if the agents are moving toward each other. This angle dependency is chosen because even if the distance between an agent-pair is short, but the airplanes fly away from each other in opposed directions, the repulsive potential should be small while the attractive potential should be large. A simple example of this behavior is illustrated in Figure 4.3. If the agents fly with equal heading angles, the repulsive and attractive potentials appear as in Figure 4.1.

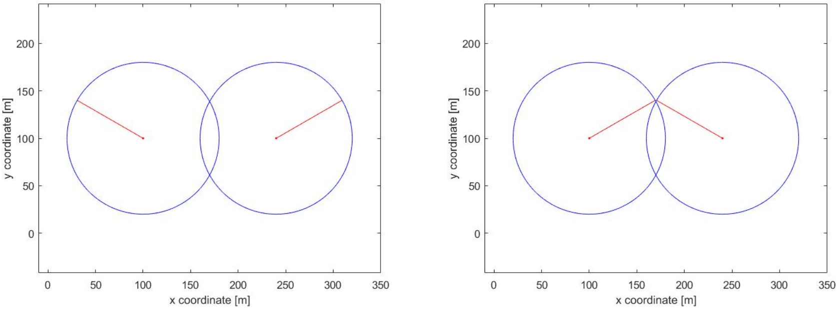

Figure 4.3 Two different setups of an agent pair. The red dots illustrate the center of the aircraft, the red lines illustrate their heading angles, and the blue circles illustrate the camera coverage. The distance between the UAVs are equal in both figures, but to prevent collision, the repulsive potential is much greater in the right figure. To ensure that the entire area between the UAVs are always covered, the attractive potential is greater in the left figure.

The repulsive potential from obstacles is inversely proportional to the approaching angle, i.e. the potential is greater for obstacles straight ahead than for obstacles parallel to the aircraft, see Figure 4.4. This angle dependency is chosen because when an aircraft is close to an obstacle but is moving away from it, there is no risk of collision and the potential should therefore decrease. For a set distance, the risk of collision is always greater when the obstacle is straight ahead of the aircraft. A sensor for obstacle detection is chosen such that obstacles can only be found within a circular sector with a limited central angle, aligned with the heading angle of the aircraft.

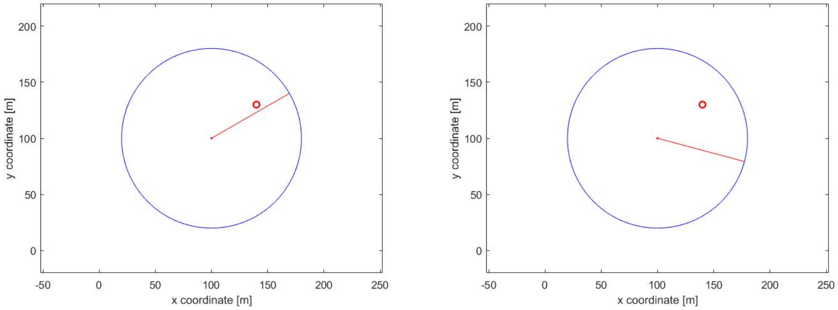

Figure 4.4 Two illustrations of a UAV and an obstacle. The red dot illustrates the center of the aircraft, the red line illustrates the heading angle, and the blue circle illustrates the camera coverage. The small red circle is a static obstacle. The distance between the UAV and the obstacle is equal in both figures, but to prevent collision, the repulsive potential from the obstacle is much greater in the left figure. There is no risk of collision in the right figure.

The attractive potential from unscanned cells is also proportional to the angle to the cell, with the UAV's heading angle as a reference. Oscillations in the flight path might occur if all unscanned cells at a certain distance have equal attractive potential, while the implementation of greater potentials for cells straight ahead reduces this risk.

5

Introduction to WPAN

There is a growing desire to use UAVs as elements in ad-hoc communication networks. Recent developments of autonomous UAVs and wireless sensor networks (WSNs) allow automated approaches to surveillance applications. A wireless backbone can be built where each UAV is equipped with a communication module. By the use of a wireless network, the UAVs can communicate with each other and with various entities on the ground with the aim of collaborating on a common task. To enable communication between any two UAVs using multi-hop ad-hoc routing, the UAVs need to maintain a fully connected network at all times [Huang and Zeng, 2007]. When designing multi-agent networks an understanding of basic radio principles is required. This chapter is intended to give an introduction to WSN technologies and starts with a short introduction to different network protocols followed by different positioning techniques.

5.1 Wireless Network Protocols

Decentralized communication can be based on a multitude of different techniques, such as Wi-Fi, Bluetooth, and ZigBee. Wi-Fi provides higher data rate than Bluetooth and ZigBee, and can operate at either a 2.4 GHz or a 5 GHz frequency band.

Bluetooth operates at a 2.4 GHz frequency band and is intended to enable short-range communications. Bluetooth transmits data via low-power radio waves and is generally used for cable replacements to connect devices such as keyboards, mice, printers, hands-free headsets, etc.

ZigBee operates at 2.4 GHz worldwide, and additionally at 900 MHz in North America and at 868 MHz in Europe. ZigBee devices are low-rate WPAN specifications and use minimal power. It can be contrasted with other approaches, such as WiFi, which offers more bandwidth and requires more power. Compared to Bluetooth, ZigBee operates well across multiple rooms. ZigBee is used mainly for battery-powered applications where low data rate, low cost, and long battery life are main requirements [Laboid et al., 2007]. ZigBee provides the most power and cost-efficient solution compared to Bluetooth and Wi-Fi and is therefore chosen to be used in this thesis. The standard protocol for ZigBee modules is further described in the upcoming subsection.

The IEEE 802.15.4 Standard

The IEEE 802.15 is the *Institute of Electrical and Electronics Engineers* (IEEE) working group that defines standards for wireless personal area networks (WPANs). More specific, IEEE 802.15.4. is a low-rate WPAN that deals with low data rate, but long battery life and low complexity. The standard defines both layer 1 and 2 in the Open Systems Interconnection model (OSI model), i.e. physical and data link layer. A common way to establish a communication network is to use the concept of networking layers where each layer holds responsibility for certain functions. This standard focuses on short-range low-cost communication between devices with little to no underlying infrastructure. See the documentation for the IEEE standard for a more in-depth description.

5.2 Sensor Networks

Localization in sensor networks is an application within sensor fusion theory using range and angle measurements. A wireless sensor network (WSN) assumes that at least two nodes exchange information using a wireless link. Wireless communication is subject to bandwidth limitations and nontrivial synchronization issues. There are three different types of observation models depending on the nodes' synchronization and communication capabilities. These observations are subject to the signal waveform, the time of arrival, and the signal power. This section further describes how different types of observations are used in localization applications.

WPAN and Positioning

There are multiple methods used for localization applications, where a few different techniques for WPAN RF modules are MAC-addresses, TOA, TDOA, RSS, and RTT.

Time of Arrival

If a transmitter and a receiver are synchronized in time, the time difference between when a message is sent and when it is received may be used to compute the distance between the devices. However, the time differences involved are usually very short, requiring the time synchronization to be precise. Each receiver measures the arrival time of a transmitted signal from an unknown position, using accurate and synchronized clocks. If the transmitter is also synchronized, the signal propagation time can be computed. The signals travel at the speed of light c, and from the propagation time t, the distance d is easily computed by the equation for non-accelerated motion.

$$d = c \cdot t \tag{5.1}$$

With TOA measurements, each receiver measurement constrains the transmitter position to a circle. A minimum of three receivers is required for 2-D positioning and a minimum of four receivers for 3-D positioning.

Time Difference of Arrival

If only the transmitters are synchronized and not the measuring device, the time difference between signals arriving from different transmitters can be measured in order to determine the position. This method can be used when the transmitter is asynchronous, but it requires the same type of time synchronization as the TOA method. Each pair of receivers computes a time difference and instead of constraining the transmitter to a circle, each pair of measurements constrains the transmitter position to a hyperbola. Four receivers compute six such hyperbolic functions, which intersect at one unique point [Gustafsson, 2012].

Round Trip Time

A way to eliminate the requirement of synchronized signals is to measure the time it takes for a message to travel to the transmitter and back again. This time is called the round trip time (RTT). As only one device performs the time measurement, the need for synchronization is eliminated. However, the time from when a device receives a message until it sends the response has to be known. Active radar, lidar, and sonar sensors emit a pulse and use RTT in order to measure range.

Received Signal Strength Indication

Most 802.11 and 802.15.4 radio modules support received signal strength indication (RSSI), which enables the calculation of the received power of each received packet. If the emitted power is known, the RSS value provides course range information. Otherwise, two or more sensors can compare their RSS observations to eliminate the unknown emitted power. Measuring the signal strength from a transmitter gives a rough indication of the distance between the modules. Multiple transmitters may then be used in order to estimate a position by multilateration.

To use RSSI for position estimation, the model needs to possess two properties. First, it needs to predict the mean signal strength at a specific distance with satisfactory precision. Secondly, the variance around the mean should be sufficiently small. There are a few different approaches to achieve this goal. One is to try to characterize the environment where the positioning is taking place, using measurements of the signal environment on numerous points. This is feasible only when the environment is either known or fairly uniform, as the resulting model is an approximation for the entire environment.

Another approach is to create a signal strength map of the environment, by a large set of measurements. This is called fingerprinting and overcomes the problem of having a changing environment [Wen et al., 2016]. However, it is impractical if used in large areas as well as when the UAVs need to be deployed quickly in an unknown area.

A third way of finding a model for the environment is to try to estimate the model parameters while the positioning is ongoing. This requires that at some point during the positioning, the position error is known to be small. Using this knowledge, suitable model parameters can be calculated. Estimating the model has the advantage of not being tied to a specific environment and whilst staying in the same environment the model will continue to improve. On the other hand, it may not produce the best results, especially when moving between different environments or if small position errors are rare or hard to distinguish.

RSSI typically does not allow to obtain positioning of high accuracy and noisy measurements give a rather large uncertainty. The frequency band of 2.4 GHz makes the measurements sensitive to interference from other devices, such as microwave ovens, cordless phones, etc.

The main advantage of using this technique is that no specific ranging devices are required other than RF communication modules. Using no extra hardware restricts the costs of the UAVs, as well as keeps the payload to a minimum.

This thesis focuses on RSSI WPAN and the positioning technique for UAV's is further explained in Chapter 7.

6

Radio Signal Propagation

Radio signal properties fundamentally limit the performance of wireless communication networks. These properties vary greatly depending on the environment the signal travels through, from a simple line-of-sight (LOS) to a severely obstructed one. As a signal travels through a wireless channel, it is generally affected by several propagation mechanisms, such as reflection, diffraction, absorption, and scattering. These phenomena lead to both large and small scale propagation losses. Obstacles such as buildings, trees, and mountains generally distort the signals on a large scale. Reflections from surfaces and absorption, diffraction, and Doppler shift due to a difference in speed between the receiver and the transmitter are small-scale affects [Rappaport, 1996].

This thesis focuses on obtaining models for outdoor propagation of radio signals in the frequency range of 2.4 GHz for outdoor positioning applications. In this chapter, a free space propagation model is presented and the concepts of antennae and receiver sensitivity are discussed. Signal propagation is introduced as well as different sources of disturbances and their influences.

6.1 Free Space Propagation Model

A transmitter equally radiating a power of P_t in all directions at a frequency of f Hz will generate a finite amount of power at a distance of d m. The received power P_r can be calculated by the use of Friis free space equation,

$$P_r(d) = \frac{P_t G_t G_r \lambda^2}{(4\pi)^2 d^2 L} \tag{6.1}$$

where P_t is the transmitted power and G_r and G_t are the antenna gains of the receiving and transmitting antenna, respectively. L is the system loss factor and is related to hardware losses only, such as line attenuation, antenna losses, and filter losses. The antenna gain is related to the effective aperture of the antenna, A_e, which in turn is dependent upon the physical size of the antenna, see the equation below.

$$G = \frac{4\pi A_e}{\lambda^2} \tag{6.2}$$

The fields of an antenna can be classified into two regions, the *far field* and the *near field*. Friis equation holds true only when the distance between the transmitter and receiver is beyond the far field distance, d_f. This distance depends upon the largest physical dimension, D, of the antenna as expressed in (6.3).

$$d_f = \frac{2D^2}{\lambda} \tag{6.3}$$

To be defined in the far field region, the following must be obtained,

$$\begin{aligned} d_f &>> D \\ d_f &>> \lambda \end{aligned} \tag{6.4}$$

where λ is the wavelength of the signal, which also can be expressed by the frequency,

$$\lambda = \frac{c}{f} \tag{6.5}$$

where c is the speed of light in vacuum in meters per second. The antennae used in this thesis have a dimension of $D < 0.04$ m. The frequency of the radio signals is 2.4 GHz, which equals a wavelength of approximately 12.5 cm. Since the distance between the receiver and the transmitter is significantly greater than the antenna dimension and the wavelength of the signal, both (6.3) and (6.4) are fulfilled.

6.2 Receiver Sensitivity

The receiver sensitivity is the lowest power level at which the receiver can detect an RF signal and demodulate data. Sensitivity is purely a receiver specification and is unaffected by the transmitter characteristics. As the signal propagates away from the transmitter, the power density of the signal decreases, making it more difficult for a receiver to detect it. Improving the sensitivity of the receiver will allow it to detect weaker signals, which may dramatically increase the transmission range. Sensitivity plays an important role in the module decision-making process since even slight differences in sensitivity can account for large variations in range.

6.3 Antennae

Different types of antennae propagate signals in different patterns. A wire or a whip antenna has omnidirectional propagation, see Figure 1. The omnidirectional propagation provides easier signal strength computations and therefore, wire antennae are used in this thesis. Any conductor of length $\lambda/4$ exposed in free space over a ground plane with a proper feed can be an effective antenna. The wire antenna gives the best performance and RF range because of its dimensions and 3-D exposure.

A PCB antenna is a trace drawn on a PCB and can have different shapes depending on the antenna type and space constraints. This antenna becomes a 2-D structure in the same plane as the PCB. It is cheaper than the wire antenna but requires more space on the PCB and has lower efficiency.

See the radiation pattern for different types of antennae in Figure 6.1.

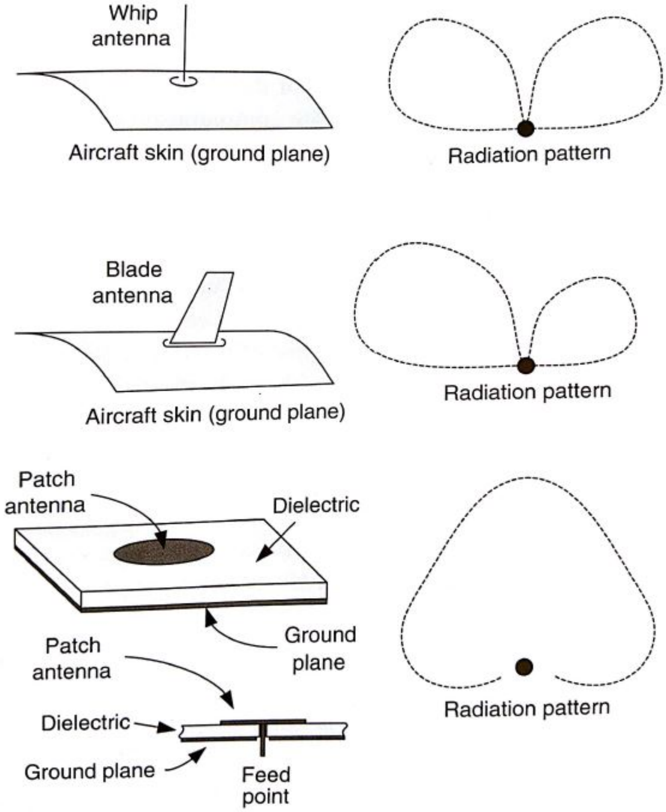

Figure 6.1 The radiation patterns of wire, blade, and patch antennae. (Reprinted with permission from [Atkins et al., 2016]. ©John Wiley and Sons.)

For wire antennae, the radio wave transmits power uniformly in all directions in one plane, with the radiated power decreasing with the elevation angle above or below the plane. In a spherical coordinate system, the two angles of elevation and azimuth are presented. The radiation is equal across the azimuthal angle, but varies with respect to the elevation angle. The radiation reaches its minimum along the axis of the antenna.

The wire antennae are the best antennae to use in terms of RF range, directivity, and radiation pattern. It is the simplest and cheapest antenna type, with low gain but good all-round coverage. A disadvantage of the wire antennae is that they tend to bend at high-speed, distorting their polar pattern. The blade antenna is a more aerodynamic form of an omnidirectional antenna.

Antenna Location

A common problem with locating antennae on an aircraft is that in certain directions the signal path may be obstructed by the airframe. Diffracted and reflected signals can create complex interference patterns, and the radiation pattern of a mounted antenna is often difficult to accurately predict. The interested reader is referred to [Atkins et al., 2016] for a detailed description on this topic.

6.4 Signal Propagation Disturbances

Radio waves are affected by the phenomenon of reflection, refraction, diffraction, absorption, polarization, and scattering. Their impact on the propagation model is further described below.

Reflection

A variety of surfaces can reflect radio signals. When radio waves are reflected, there is generally some loss of the signal, either through absorption or as a result of when a part of the signal is passing through the medium. For long-distance communications, the sea is a common source of reflection. Similarly, buildings and other metallic structures provide excellent reflectors for relatively short-range communications. In general, when a radio wave propagates from one medium to another medium with a different set of electrical properties, the wave is partially transmitted and partially reflected. The intensities of the transmitted and the reflected part depend on the material properties, the wave polarization, the angle of incident, and the frequency of the wave. For a surface to be considered as a possible source of reflection, the requirement is that its dimensions are much larger than the signal's wavelength [Rappaport, 1996].

Diffraction

Diffraction occurs when the signal path is blocked by an object which causes the waves to bend around the obstacle. This phenomenon is also known as *shadowing* and is caused by secondary wavelets that propagate into a shadowed region. Since only a fraction of the wave propagates into the shadowed region, the signal strength decays rapidly when moving further into the region.

Scattering

Scattering causes the reflected energy to spread out in many directions and occurs when radio waves are reflected on objects with dimensions smaller than the signal's wavelengths. Even flat surfaces may possess some roughness and therefore obtain scattering properties.

Multipath

Multipath propagation causes large and rapid fluctuations in a signal, as multiple waves arrive at the receiver with a phase difference. This phenomenon results in small-scale fading. Multipath waves also cause random frequency modulation due to Doppler Shifts on different multipath signals. For a more in-depth description, the interested reader is referred to [Rappaport, 1996].

7

Positioning - RSSI Approach

Most of the existing UAV positioning systems rely on the use of GPS signals. In open environments where GPS signals are available, this method generally provides satisfactory position estimates. In some areas, GPS signals are unavailable or unreliable, for example in indoor environments or in obstructed areas, such as close to high buildings and mountains. An obstructed path results in a longer distance for the signal to travel before it reaches the receiver. This increase of distance may be caused by several propagation effects, such as reflection, diffraction, or scattering. Since the distance is estimated by the time difference between when a signal is transmitted and when it is received, an obstructed path leads to an increased distance estimate. Further, as the GPS signal is sent from space, it is already relatively weak when it reaches the surface of the Earth and an obstruction may even make the signal too weak to be detected by the receiver.

In this thesis, low-cost UAVs are used in order to scan areas for surveillance applications. Since the cost of the devices involved in the positioning operations is limited, an approach based on RSS measurements is considered. Each UAV is assumed to be equipped with communication devices used to share information with other members of the swarm to improve their cooperation abilities. RSS based positioning does not require any additional hardware.

This chapter first introduces RSSI principles and different propagation models. Note that the model parameters may need to be tuned differently for specific devices as they possess different parameters. In order to use RSSI for positioning applications, sensor fusion is applied and further explained in Section 7.3.

7.1 RSSI

Received signal strength indicator (RSSI) is a measurement of the signal power of a received radio signal. The power of a signal traveling between two nodes in combination with a path-loss and shadowing model can be used for distance estimation. In this thesis, the UAVs communicate with their neighbors by single-hop messages which are periodically propagated and broadcasted to all UAVs within their communication range. This can be compared to the way birds fly in a flock, mostly using the information from neighboring birds. This locality of the communication is a simple way to keep the network scalable to changes of the swarm size.

The message may contain arbitrary content of up to 512 bytes in length. Thus, with the aid of the RSSI values of the received messages, the UAV's 2-D position can be determined by a set of at least three distance estimates, provided that the message includes the most recent position estimate of the transmitting UAV, its transmission frequency, and a time-stamp. The process is repeated until the RSSI values of all reachable transmitters have been measured.

RSSI measurements are unpredictable due to several error sources, such as time delays and multipath signals arriving at the receiver. For the RSSI to be a meaningful measurement of the received signal power it must somehow be related to the physical properties of the signal. For model evaluations, an investigation of how the RSSI changes with the distance is commonly used together with the RSSI value at a known distance. There is no standard of how the RSSI should be related to the physical properties of the signal, and manufacturers are able to choose in what range the RSSI value should be presented. RSSI is given in an arbitrary unit, usually in dBm.

7.2 Propagation Models

The majority of RSSI location algorithms make use of a signal propagation model that maps RSSI values to distance estimates. The most widely model for RSSI based position estimation for outdoor applications is the log-normal shadowing model (LNSM) [Seybold, 2005].

Log-Normal Shadowing Model

The LNSM is shown in (7.1),

$$P(d) = P(d_0) - 10\eta \log_{10}\left(\frac{d}{d_0}\right) + X_\sigma \tag{7.1}$$

where $P(d)$ is the received signal strength at distance d and $P(d_0)$ the signal strength for a reference distance d_0, commonly chosen at 1 meter for simplicity. η is the signal attenuation coefficient and X_σ is assumed to be a Gaussian random variable with zero mean and variance σ^2. η depends on the specific environment and is approximately 2 in free space and larger when obstacles are present. If d_0 is chosen to be 1 m, the corresponding distance can be computed from (7.2) as follows.

$$d = 10^{-(P(d) - P(d_0) - X_\sigma)/10\eta} \tag{7.2}$$

Due to the non-linearity in (7.2), it is clear that the effect of noise changes depending on the considered distance. The same value of X_σ leads to a much larger distance estimation error for small values of the measured signal strength, i.e. larger distances.

Double Slope Model

A simple extension of the log-normal shadowing model is to combine different values of η for various intervals of the RSSI. The most simple of these models is the double slope model where two different path loss exponents are used together with a single break value of the received power, P_1. The model then becomes,

$$d = 10^{-(P(d)-P(d_0)+X_{\sigma_1})/10\eta_1} \qquad \text{if } P(d) \geq P_1 \tag{7.3}$$

$$d = 10^{-(P(d)-P(d_0)+X_{\sigma_2})/10\eta_2} \qquad \text{if } P(d) < P_1 \tag{7.4}$$

where X_{σ_1} and X_{σ_2} are random Gaussian distributed variables with zero mean and standard deviation σ_1 and σ_2, respectively. Note that there might occur an undesirable jump in the estimated distance at P_1 when the path loss exponent is suddenly switched from one value to another.

$\alpha\beta$-Model

Another extension of the LNSM model is to introduce a parameter α multiplied by the distance d, as well as a parameter β as an exponent of this d. This expression is subtracted from the LNSM in (7.1).

$$P(d) = P(d_0) - 10\eta \log_{10}\left(\frac{d}{d_0}\right) - \alpha d^{\beta} + X_\sigma \tag{7.5}$$

For this model, an initial η is chosen and α and β are tuned in order for the model to achieve desirable results. In [Karlsson and Karlsson, 2014], an α-model is used for indoor applications (i.e. β is set to 1). This model tends to underestimate the signal strength at large distances d as α grows linearly with d while everything else grow as the logarithm of d. Two simple ways to correct for this are that either the model can be switched to a standard log-normal shadowing model when d is large, or a maximum value of αd may be imposed. The α model works better for shorter distances, such as for indoor applications. In this thesis, an attempt of adding a parameter β to improve the model accuracy is taken into consideration for the model evaluation.

7.3 Sensor Fusion

Sensor fusion deals with merging information from two or more sensors, where the goal is to achieve as accurate information as possible. The sensory data from different sensors is combined such that the resulting information is somewhat improved and more useful than when using the sources individually. For sensor fusion approaches, different filters can be applied, such as variations of the Kalman filter or a particle filter. Different filtering methods are described further in Chapter 9.

In this project, sensor fusion is used to estimate the position of the individual UAVs. All UAVs are assumed to be equipped with wireless RF modules for communication. The communication modules are sending data packages between UAVs and the received signal strength is measured in order to estimate the distance between them. The modules work in broadcast sending mode while the RSS is measured continuously. Swarm members process incoming data packages from other UAVs within their communication range. All communication is assumed to be synchronized and time delays are omitted.

Multilateration

An example of positioning is illustrated in Figure 7.1, where the blue triangles represent UAVs at known positions. Each UAV transmits its coordinates as well as heading and bank angle to a receiver at an unknown position. The solid circles illustrate the distance estimates computed from the received RSSI values. This is an example of trilateration and by applying sensor fusion the position of the receiving UAV can be estimated, illustrated as a red triangle in Figure 7.1.
Consider a UAV with unknown coordinates (p_x, p_y) and N nodes with known positions (x_n, y_n). From this, the coordinates of the UAV can be computed, given the distances d_n from the nodes to the UAV.

$$\sum_{n=1}^{N}\left(d_n - \sqrt{(x_n - p_x)^2 + (y_n - p_y)^2}\right) = 0 \tag{7.6}$$

In most cases, due to the noise and errors in RSSI measurements causing distance estimation errors, the right-hand side of (7.6) is non-zero, which leads to a non-solvable system. If this is the case, multilateration can still be used to estimate the position of the UAV, by minimizing an error function.

Consider three circles of radius d_1, d_2, and d_3 as in Figure 7.2. The dotted lines represent the distance estimation errors, which increase with increased distance.

The position can be estimated using a weighted non-linear least square filter (WNLS), see Chapter 9 for details. The goal is to minimize the following error function in order to estimate the unknown position.

$$V^{WNLS}(p) = (\mathbf{y} - \mathbf{h}(p))^T \mathbf{R}^{-1}(p)(\mathbf{y} - \mathbf{h}(p)) \tag{7.7}$$

In (7.7), $\mathbf{y}$ is the computed distance from the RSSI measurements, $\mathbf{h}$ is the distance from each AP as a function of p, and $\mathbf{R}$ is a diagonal 2x2 covariance matrix [Gustafsson, 2012].

When estimating the covariance matrix, all intersections are evaluated and if an intersecting point from d_1 and d_2 is inside all of the remaining circles, the coordinates of the point are saved in a vector. This is done for all intersection point of all

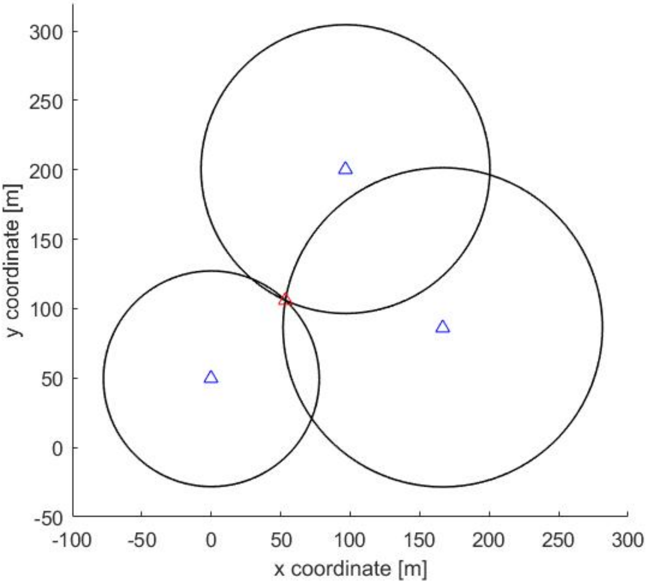

Figure 7.1 Position estimation of one unknown node using trilateration of signals from three known access points.

circles. The covariance is estimated as an ellipse over all of the points in this vector, see Figure 7.3. The ellipse is chosen such that it covers a certain percent of the area of the position uncertainty. At the same time, the ellipse minimize its coverage of unwanted areas.

The confidence bounds for the position is computed using a normal approximation to the distribution of the estimate.

$$\frac{X - \hat{\mu}}{\hat{\sigma}} \tag{7.8}$$

The normal cumulative distribution function (cdf) is

$$p = F(x|\mu, \sigma) = \frac{1}{\sigma\sqrt{2\pi}} \int_{-\infty}^{x} e^{\frac{-(t-\mu)^2}{2\sigma^2}} dt \tag{7.9}$$

where p is the probability that a single observation from a normal distribution with parameters μ and σ will fall in the interval $(-\infty\ x]$.

All x and y values in the vector are subtracted by the position estimate, and this new vector is denoted as X_0. A confidence interval is chosen based on the desired standard deviation. From this, the inverse of the 2 degree of freedom χ^2 cdf is

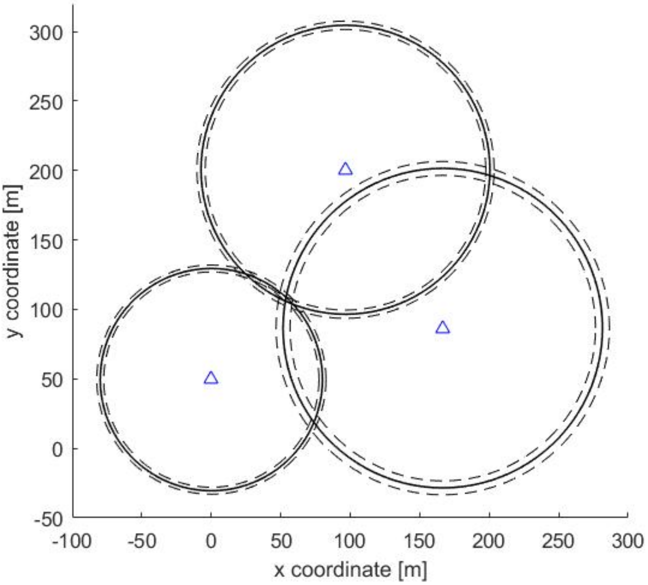

Figure 7.2 Position estimation of one unknown node using trilateration of signals from three known access points with position uncertainties. For a zoomed in picture of the circle intersections, see Figure 7.3.

computed and further multiplied by the covariance of X_0. The resulting matrix is the covariance ellipse used for the position estimate.

Depending on the intersecting points, the ellipse might not always provide a satisfactory estimate of the covariance. The covariance does not attain the shape of an ellipse and for this approach, there has to be a trade-off between the missed area and the unwanted area covered.

Sequential Localization

The position estimation technique described in the previous section can be applied sequentially to each agent in a swarm. One agent receives incoming packets from nearby agents, who all broadcast their latest updated position. The error cost function in (7.7) is applied for each position estimation update. All UAVs are considered to be at known stationary positions when the position estimate is computed. Time delays for signal transmission and package handling are not taken into consideration.

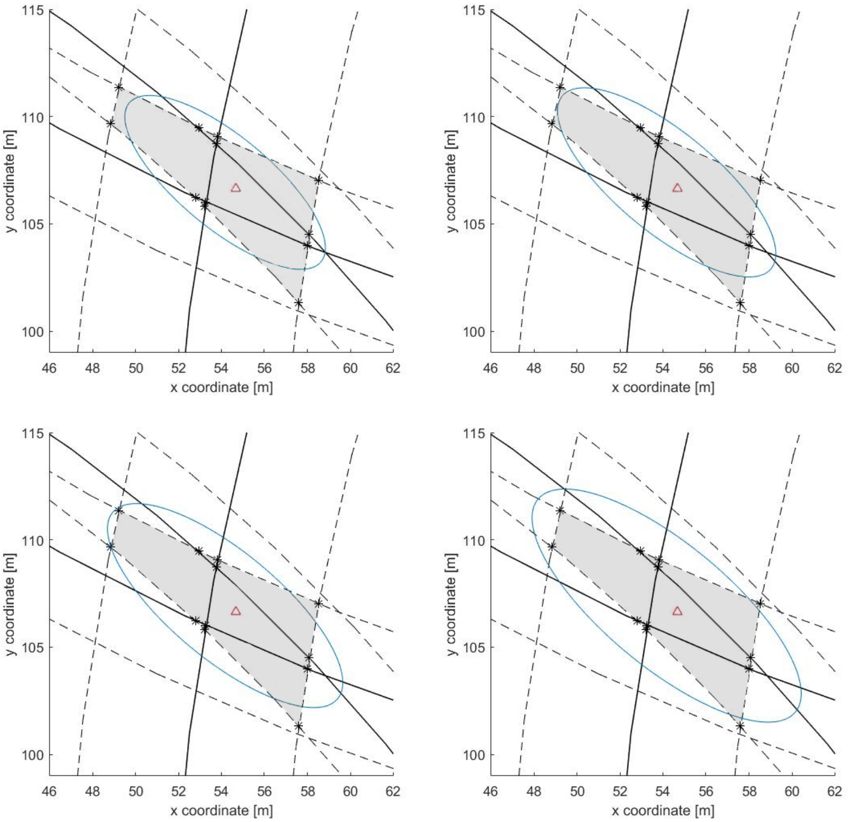

Figure 7.3 Position and covariance estimates using trilateration. The black solid lines represent the estimated distances from known positions and the dotted lines are the uncertainty of the estimates. The red triangles represent the position estimate from multilateration using WNLS. The stars are positioned at the intersection points which are located within all three circles from Figure 7.2. The grey area within these intersection points is the covariance of the position estimate. The blue ellipse is an estimation of the covariance **R**. The standard deviation increases from the upper left corner to the bottom right.

8

Aircraft Kinematics and Dynamics

Modeling the kinematics will greatly improve the position estimates, since outliers of the RSSI measurements, which result in false position estimates, will be filtered out. In this chapter, a short introduction to aerodynamics is presented and kinematics for a 2-D UAV is further explained. When the UAVs are in motion, the difference in signal strength between two RSSI measurement updates is limited, depending on the speed, acceleration, and heading angle of the aircraft. If the change in RSSI exceeds this value, the signal path is most likely obstructed, or somehow disturbed, and the RSSI should not be trusted.

8.1 Aerodynamics

Flight dynamics describe the orientation and control of an aircraft in three dimensions. The critical parameters of the flight dynamics are the angles of rotation about the aircraft's center of mass, known as pitch, roll, and yaw, see Figure 8.1. These angles are referred to as Euler angles and describe the orientation of a rigid body with respect to a fixed coordinate system. The Euler angle representation has a singularity when the pitch angle is ±90 degrees. Physically, when the pitch angle is 90 degrees, the roll and yaw angles are indistinguishable. This singularity is not an issue for the vast majority of flight conditions unless acrobatic flights or other extreme maneuvers are performed. Quaternions provide an alternative way of presenting the attitude of an aircraft and does not have any singularity issues. A throughout description of quaternions and rotation sequences is given in [Kuipers, 1999]. However, since the aircraft in the simulations of this thesis fly at a constant altitude and the pitch angle is assumed to be zero, singularity issues will not arise with the Euler angle representation.

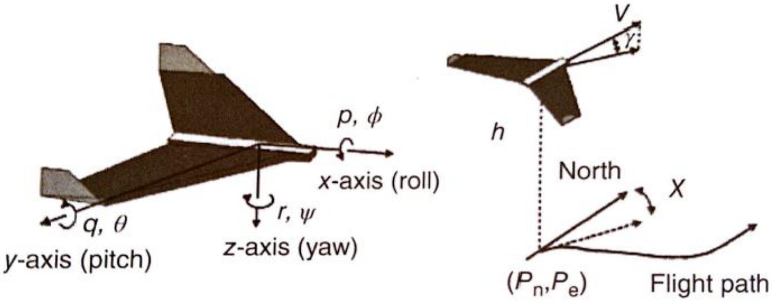

Figure 8.1 Definition of the variables used throughout this chapter. The angular rates are given by p, q, and r, and the Euler angles are denoted as ϕ, θ, and ψ. V represents the airspeed, the heading angle is χ, and the flight path angle is γ. The inertial position in 2-D is (p_n, p_e) and the altitude of the aircraft is h. (Reprinted with permission from [Atkins et al., 2016]. ©John Wiley and Sons.)

The Euler angles can be estimated by integrating the rate gyros, where accelerometers may be used to correct for integration constants and biases and drift in gyro. The derivatives of the three Euler angle states in terms of the angular positions and the body rates are expressed in (8.1).

$$\begin{pmatrix} \dot{\phi} \\ \dot{\theta} \\ \dot{\psi} \end{pmatrix} = \begin{pmatrix} 1 & \sin\phi\tan\theta & \cos\phi\tan\theta \\ 0 & \cos\phi & -\sin\phi \\ 0 & \sin\phi\sec\theta & \cos\phi\sec\theta \end{pmatrix} \begin{pmatrix} p \\ q \\ r \end{pmatrix} \tag{8.1}$$

A rudder is located on the vertical tail fin of the aircraft and is used to control the yaw angle. The rudder is turned in the direction of which the aircraft should turn. Ailerons are located on the outer rear edge of each wing and control the roll angle. The two ailerons move up and down in opposite directions, decreasing lift on one wing while increasing it on the other. Usually, the rudder is used along with the ailerons to turn an airplane. The elevator controls the pitch angle and is positioned on the horizontal tail surface. The elevator tilts up or down, decreasing or increasing lift on the tail.

The turning radius R of an aircraft is given by

$$R = \frac{V_g \cos\gamma}{\dot{\chi}} = \frac{V_g^2 \cos\gamma}{g\tan\phi\cos(\chi-\psi)} \tag{8.2}$$

where γ is the flight path angle which is assumed to be zero in the simulations due to a constant altitude. V_g is the ground speed, which is equal to the airspeed V in the absence of wind. χ is the the coarse angle from North to the projection of V onto a horizontal plane. When no wind is present, the sideslip angle is neglected and the coarse angle is equal to the yaw angle. In the absence of wind, (8.2) is simplified to equal the expression in (8.3). The relationship between airspeed, wind speed, and ground speed is illustrated in Figure 8.2.

$$R = \frac{V_a^2}{g \tan \phi} \tag{8.3}$$

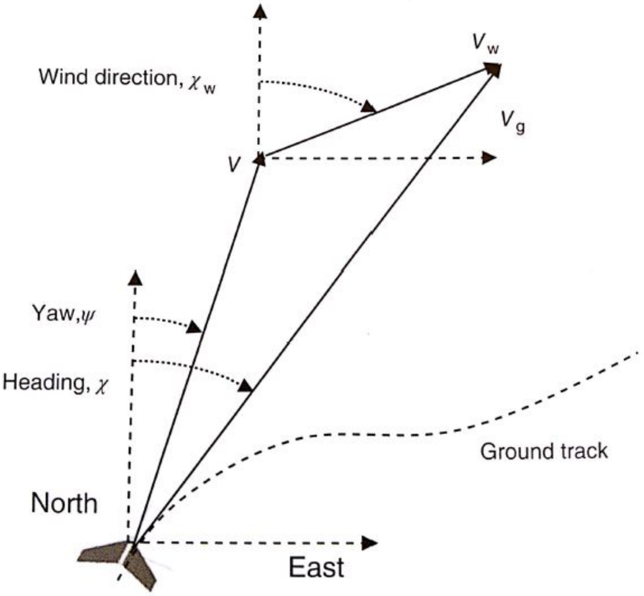

Figure 8.2 This figure shows the relationship between the airspeed V, the wind speed V_w, and the ground speed V_g, as well as the relationship between yaw ψ, heading χ, and wind direction χ_w. The crab angle is defined as the heading minus the yaw. (Reprinted with permission from [Atkins et al., 2016]. ©John Wiley and Sons.)

For an aircraft in a coordinated turn (i.e., no skidding or slipping), the vertical component of lift equals the weight of the aircraft, while the horizontal component equals the centrifugal force. The coordinated turn condition in the absence of wind is presented in (8.4).

$$\dot{\psi} = \frac{g}{V} \tan \phi \tag{8.4}$$

The simulations are based on a 2-D model and for simplicity, the yaw angle is controlled directly and not via the roll angle. The value of the roll angle can be computed through a second order differential equation, see details in [Beard and McLain, 2012].

The term *bank angle* is used for a stable roll and is not an instantaneous roll state. If an aircraft dwells in a roll angle in a stable way for some time, it is called bank angle. A relationship between the minimum turning radius and the maximum bank angle for different airspeeds is seen in Figure 8.3. As the aircraft turns with a constant bank angle and the airspeed increases, the turning radius increases with the square of the speed. In other words, the distance traveled during the turn increases with the square of the speed.

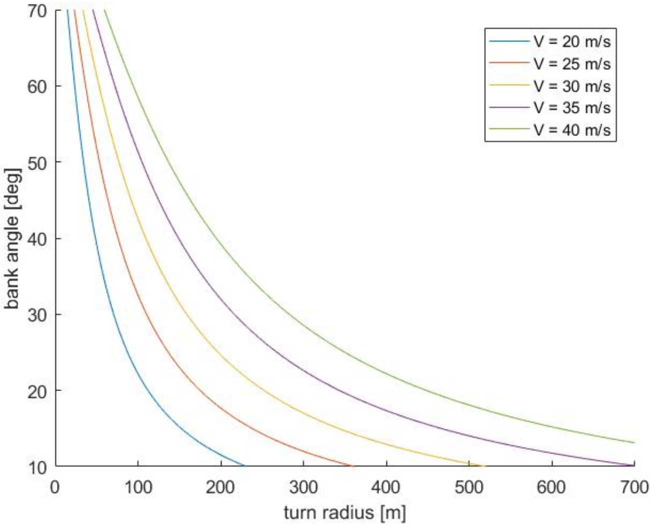

Figure 8.3 Bank angle versus turning radius for a small unmanned vehicle. For a fixed bank angle, an increase of airspeed leads to a greater turning radius.

The acceleration required in order to keep an aircraft circulating at a constant altitude is expressed in (8.5).

$$a = \frac{V^2}{R} \tag{8.5}$$

The load factor n depends on the airspeed, the bank angle, and the turning radius. How these parameters are related can be seen in Figure 8.4 and is mathematically expressed in (8.6).

$$n = \frac{\sqrt{g^2 + a^2}}{g} = \frac{a}{g \sin\phi} = \frac{V^2}{Rg \sin\phi} \tag{8.6}$$

As seen in (8.6) and in Figure 8.5, the load factor increases with an increased bank angle. The steeper the bank, the greater the centrifugal force, hence the higher the load factor. If the roll angle is zero, there is no centrifugal force, i.e. both ϕ and a are zero and the load factor is 1 as expected from (8.6). The bank angle is chosen to be limited in the simulations due to the receiver sensitivity of the communication devices, see Chapter 10 for further explanation. A limited bank angle results in a limited load factor. Figure 8.6 illustrates the airspeed as a function of turning radius for different values of the load factor.

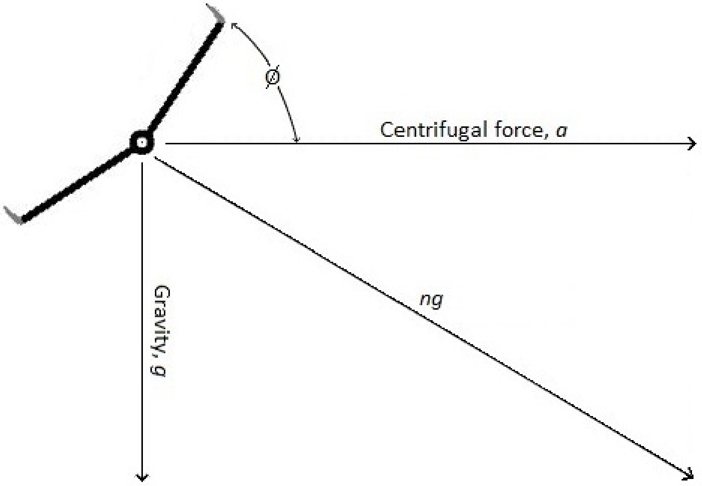

Figure 8.4 Forces acting on an aircraft during a level coordinated turn, where n is the load factor and ϕ is the roll angle.

8.2 Kinematic Model

Since the simulated aircraft maintain a fixed altitude a 2-D model is applied. For this approach, the yaw angle is the only angle of interest and the other Euler angles are chosen not to be modeled. With that said, note that the roll angle is non-zero when the aircraft makes a turn, i.e. when $\dot{\psi} \neq 0$, but for simplification, this angle is chosen not to be a part of the dynamic model. In this section, the concept of dead reckoning is presented, followed by an explanation of the 2-D dynamic model used in the simulations.

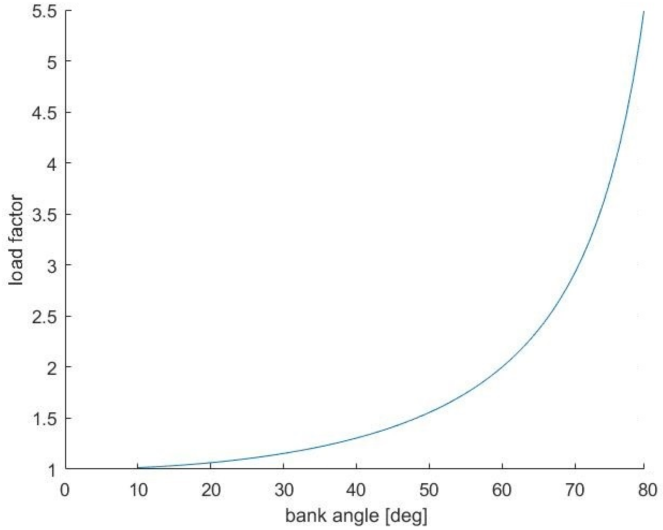

Figure 8.5 Load factor *n* as a function of the bank angle in degrees.

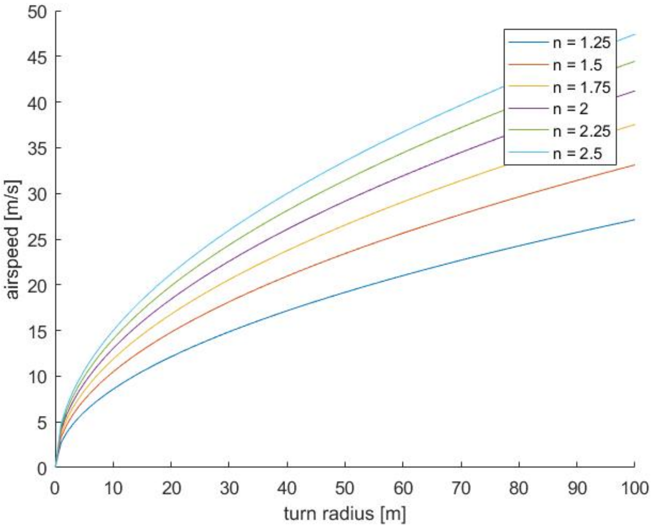

Figure 8.6 Airspeed *V* as a function of turning radius *R* for different load factor values *n*.

Dead Reckoning

One of the oldest methods of navigation is dead reckoning (DR) which relies on the measurements of heading and longitudinal speed. This position estimation technique is suitable for larger vehicles, such as aircraft or ships. In order to measure speed and heading, this approach generally uses accelerometers and gyroscopes. The estimated position from the previous time step is used to compute the current position. If the estimated heading is ψ and the estimated airspeed is V, the change in Cartesian coordinates is the following,

$$\begin{aligned} \dot{x} &= V \cos \psi \\ \dot{y} &= V \sin \psi \end{aligned} \tag{8.7}$$

Note that this simple model is not valid when the vehicle is exposed to sideslip. Suppose that the change in heading is estimated from an angular rate gyroscope,

$$\dot{\psi} = r \tag{8.8}$$

where r is the measured angular rate, earlier mentioned in Figure 8.1. Integration of rate gyros is subject to drift and the error from dead reckoning grows over time. In order to correct for this, sensor fusion with an accelerometer and a magnetometer can be implemented. Dead reckoning generally works well for short distances and can be applied when the information from position measurements is distorted. In this thesis, dead reckoning is used to estimate the position when not enough RSSI measurements are available and when the RSSI measurements are unreliable.

2-D UAV Dynamic Model

The pose of an aircraft is defined by $[x\ y\ \psi]^T$, where x and y are the UAV's Cartesian coordinates and $\psi \in (-\pi,\ \pi]$ is the heading angle with $\psi = 0$ lying on the x-axis. The position and orientation of a UAV change via the on-board control loop, which defines the UAV's linear acceleration $\dot{V}$ and angular velocity $\dot{\psi}$.

The discrete-time dynamic model of the UAVs is given in state space form in (8.9).

$$\mathbf{x}_k = \begin{pmatrix} x_{1,k} \\ x_{2,k} \\ x_{3,k} \\ x_{4,k} \end{pmatrix} = \begin{pmatrix} x_k \\ y_k \\ V_k \\ \psi_k \end{pmatrix} \tag{8.9}$$

The state updates are described in Equation (8.10) and (8.11), where the subscript *des* stands for *desired* which is used as a reference value.

$$\begin{pmatrix} x_{k+1} \\ y_{k+1} \\ V_{k+1} \\ \psi_{k+1} \end{pmatrix} = \begin{pmatrix} x_k \\ y_k \\ V_k \\ \psi_k \end{pmatrix} + \begin{pmatrix} T_s \cdot V_k \cdot \cos \psi_k \\ T_s \cdot V_k \cdot \sin \psi_k \\ V_{k+1_{des}} - V_k \\ \psi_{k+1_{des}} - \psi_k \end{pmatrix} + \begin{pmatrix} 0 \\ 0 \\ w_{V,k} \\ w_{\psi,k} \end{pmatrix} \tag{8.10}$$

In (8.10), the speed update V_{k+1} and the heading angle update ψ_{k+1} hold true if $|V_{k+1_{des}} - V_k| \leq T_s \cdot \dot{V}_{max}$ and $|\psi_{k+1_{des}} - \psi_k| \leq T_s \cdot \dot{\psi}_{max}$, respectively. If these criteria are not met, the speed and heading angle states are updated according to (8.11). The control variables are modelled with the zero-mean white noise $w_{V,k}$ and $w_{\psi,k}$. These parameters represent model uncertainties and unmodeled dynamics.

The desired speed and yaw angle are computed from the attractive and repulsive potential functions described in Chapter 4. The derivative of V and ψ are limited by maximum acceleration and turning rate, respectively.

$$\begin{pmatrix} V_{k+1} \\ \psi_{k+1} \end{pmatrix} = \begin{pmatrix} V_k \\ \psi_k \end{pmatrix} + T_s \begin{pmatrix} \operatorname{sign}\left(V_{k+1_{des}} - V_k\right) \cdot \dot{V}_{max} \\ \operatorname{sign}\left(\psi_{k+1_{des}} - \psi_k\right) \cdot \dot{\psi}_{max} \end{pmatrix} + \begin{pmatrix} w_{V,k} \\ w_{\psi,k} \end{pmatrix} \tag{8.11}$$

The first row of (8.11) holds true if $|V_{k+1_{des}} - v_k| \geq T_s \cdot \dot{V}_{max}$ and the second row if $|\psi_{k+1_{des}} - \psi_k| \geq T_s \cdot \dot{\psi}_{max}$. The acceleration is limited in the simulations due to a limitation in load factor and maximum bank angle from RSSI measurements, see details in Chapter 10.

9

Filters

Filtering plays an important role in signal processing applications and is widely used in many fields within communication, electronics, image processing and computer graphics. Filters are commonly used in order to remove unwanted frequencies or certain features from a signal or to estimate unknown states. In this chapter, multiple filtering techniques are further discussed.

9.1 Non-Linear Filtering Theory

A dynamic system can in general terms be characterized by a state space model, where $\mathbf{x}_k$ are the states and $\mathbf{y}_k$ represents the observations at time k. The following equation is the most common non-linear state space model,

$$\begin{aligned} \mathbf{x}_{k+1} &= \mathbf{f}(\mathbf{x}_k, \mathbf{u}_k, \mathbf{w}_k) \\ \mathbf{y}_k &= \mathbf{h}(\mathbf{x}_k, \mathbf{u}_k) + \mathbf{e}_k \end{aligned} \tag{9.1}$$

where the process and measurement noise, $\mathbf{w}$ and $\mathbf{e}$ respectively, are random processes with arbitrary probability density functions (pdf's). The control input $\mathbf{u}$ is a known input to the system and often omitted. For filtering applications related to this thesis, $\mathbf{x}$ commonly include position, velocity, and acceleration. $\mathbf{y}$ are observations obtained by either onboard or external sensors. Multiple states may be unknown, where partial information is obtained by observations. Non-linear filtering problems make inference on the state from the observations.

There are multiple methods for solving filtering problems, where one of the most common is the Kalman filter. If either one of $\mathbf{h}$ or $\mathbf{f}$ is non-linear, an extended Kalman filter (EKF) needs to be applied. Kalman Filters assume that both the measurement and process noise are zero-mean Gaussian. Kalman filters also require the posterior distribution of the states to be zero-mean Gaussian.

The particle filter, also called sequential Monte Carlo method, is a simulation-based approach for solving estimation problems. This method does not require Gaussian noise, as long as the probability density functions of $\mathbf{e}$ and $\mathbf{w}$ are known, but suffer from high computational complexity.

Extended Kalman Filter

An extended Kalman filter is an optimal estimator which combines parameters of interest from indirect, inaccurate, and uncertain observations. The EKF is a recursive algorithm as new measurements can be processed as they are available. Equation (9.2) to (9.9) show the time and state update for a discretized extended Kalman filter. $\mathbf{x}_k$ is the state at time k. $\mathbf{w}_k$ is the process noise which is assumed to be drawn from a zero mean multivariate normal distribution with covariance $\mathbf{Q}_k$. Non-modeled dynamics and parameter uncertainties are generally modeled as process noise. $\mathbf{v}_k$ is the measurement noise which is assumed to be zero mean Gaussian white noise with covariance $\mathbf{R}_k$.

$$\hat{\mathbf{x}}_{k+1|k} = \mathbf{f}(\hat{\mathbf{x}}_k, 0, 0) \tag{9.2}$$

$$\mathbf{P}_{k+1|k} = \Phi_k \mathbf{P}_{k|k} \Phi_k^T + \Gamma_k \mathbf{Q}_k \Gamma_k^T \tag{9.3}$$

$$\Phi_k = \frac{\partial \mathbf{f}(\hat{\mathbf{x}}_k, 0, 0)}{\partial \mathbf{x}_k} \tag{9.4}$$

$$\Gamma_k = \frac{\partial \mathbf{f}(\hat{\mathbf{x}}_k, 0, \hat{\mathbf{w}}_k)}{\partial \mathbf{w}_k} \tag{9.5}$$

$$\mathbf{H}_{k+1} = \frac{\partial \mathbf{h}_{k+1}(\hat{\mathbf{x}}_{k+1|k}, 0)}{\partial \mathbf{x}_{k+1}} \tag{9.6}$$

$$\mathbf{K}_{k+1} = \mathbf{P}_{k+1|k} \mathbf{H}_{k+1}^T (\mathbf{H}_{k+1} \mathbf{P}_{k+1|k} \mathbf{H}_{k+1}^T + \mathbf{R}_{k+1})^{-1} \tag{9.7}$$

$$\hat{\mathbf{x}}_{k+1|k+1} = \hat{\mathbf{x}}_{k+1|k} + \mathbf{K}_{k+1}(\mathbf{y}_{k+1} - \mathbf{h}_{k+1}(\hat{\mathbf{x}}_{k+1|k}, 0)) \tag{9.8}$$

$$\mathbf{P}_{k+1|k+1} = (\mathbf{I} - \mathbf{K}_{k+1} \mathbf{H}_{k+1}) \mathbf{P}_{k+1|k} \tag{9.9}$$

$\hat{\mathbf{x}}_{k+1|k}$ is an estimate of $\mathbf{x}_{k+1}$ from observations up to sample k. $\mathbf{H}$ is the measurement Jacobian and is evaluated at the current state estimate, which maps the true state space into the observed space. $\mathbf{K}$ is the optimal gain, also known as the Kalman filter gain and minimizes $\mathbf{v}\mathbf{P}\mathbf{v}^T$ for any vector $\mathbf{v}$. $\mathbf{I}$ is the identity matrix and the covariance matrix of the measurement noise is denoted as $\mathbf{R}$. Even if the measurement noise is perfectly Gaussian, its impact on the state estimate is not, due to the non-linearity in the measurement function, but the EKF does not account for this. $\mathbf{Q}$ is the covariance matrix for the process noise, where the diagonal contains the variance of each state variable, and off-diagonals contain the covariances between the different state variables. Practical implementations of Kalman filters in general are often difficult due to the fact that the noise matrices are seldom known a priori. These matrices are estimated and generally assumed to be diagonal, i.e. the noise is uncorrelated for the different states.

Weighted Non-Linear Least Square

Least square methods (LS) are common estimation techniques for over-determined systems. LS is based on the minimization of the error between an observed value and a modeled one. In this thesis, least square is used in the first position estimation step when fusing the distance estimates from neighboring agents. When estimating a variable, a cost function V is minimized.

$$\hat{p} = \text{argmin} V(p) = \text{argmin}||\mathbf{y} - \mathbf{h}(p)|| \tag{9.10}$$

For weighted non-linear least square, *WNLS*, the cost function V is

$$V^{WNLS}(p) = (\mathbf{y} - \mathbf{h}(p))^T \mathbf{R}^{-1}(p)(\mathbf{y} - \mathbf{h}(p)) \tag{9.11}$$

which uses the same notation for **h** and **y** as the EKF. **R** is the covariance matrix of the estimate.

Particle Filter

A particle filter (PF) provides an approximation to the posterior distribution $p(x_k|y_{1:k})$ of the state x_k conditioned on the set of measurements $y_{1:k}$, see (9.1). This approximation is based on a set of N samples, referred to as particles. The PF uses a dynamic model and recursively processes data by updating the measurement, re-sampling the step, and lastly updating time. The PF may obtain desirable results when used in position applications and performs quite well in a three-dimensional state-space consisting of horizontal position and coarse. However, the PF is not practically useful if more dynamic states are added, such as accelerometers, unmeasured velocities, etc. [Karlsson and Karlsson, 2014]. The PF is also infeasible when the model consists of motion in three dimensions or sensor biases and drifts. This results in a too sparse representation of the posterior distribution as the required number of particles grows.

10

Distance Model Evaluation

In this chapter, the experimental setup for the RSSI measurements is presented. The propagation models evaluated in Section 7.2 are further analyzed on static RSSI measurements. In reality, the RSSI value is not only dependent on the distance and angle but also influenced by the environment. The RSSI signal will contain noise caused by multipath reflections when signals bounce against objects in the environment such as ground, trees, and buildings.

When communication modules are mounted on UAVs and one UAV turns away from another, signal blockage and other propagation disturbances will occur. One way to account this is to place two communication devices on each UAV, such that one of them always is in line-of-sight with the communication devices on neighboring UAVs.

10.1 Experimental Setup

The measurements took place on a relatively flat field without trees and other obstacles. Two wire antennas are attached vertically to the PCB, initially pointing up towards the sky. The experimental setup is illustrated in Figure 10.1, where two XBees are mounted on XBee shields connected to Genuino UNOs. XBee modules have an RSSI pin that outputs a PWM signal, which represents the received signal strength. To be able to measure the RSSI at multiple distances, one of the microcontrollers is battery powered by a 9 V battery.

The second microcontroller is connected to a PC and programmed to transmit data packages with a certain repitition rate, where the mounted transmitter retransmits any data package it receives. The battery-powered XBee is constantly reading the RSSI value of the receiving data packets and sends back a message containing this value to the other XBee via the microcontroller. The XBee receiving this message reads the RSSI and saves it in a vector in MATLAB, together with the measured distance.

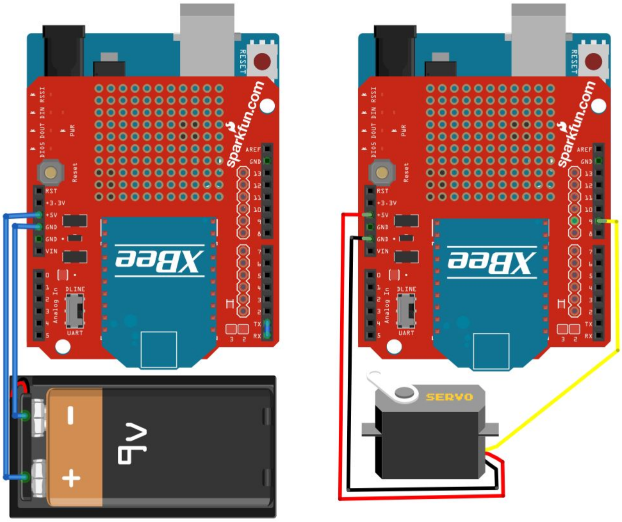

Figure 10.1 Experimental setup for RSSI measurements.

The communication devices were placed on ladders in order to avoid interference from the ground. Both the receiver and the transmitter were positioned at a height of approximately 1.5 meters above the ground. By placing the modules high, both the risk of interfering with the person taking measurements and the risk of absorption and reflection from the ground decrease. Disturbances will generally result in a weaker signal which leads to an increase in the distance estimate. In the first attempt of the experiment, the RSSI was measured when the modules were placed approximately 0.5 meters from the ground. These measurements were unreliable since significant signal disturbances occurred as the RSSI fluctuated for fixed positions.

It is also of interest to see how the RSSI values are affected by angle differences between the transmitter and the receiver. For this experiment, a servo motor is connected to the PC-powered microcontroller. The angle of the shaft of the servo motor is automatically controlled by the microcontroller, which is mounted on the servo. The transmitter rotates along its longest side and for each position, the RSSI is measured. 19 different angels, $\phi = [-90^o : 10^o : 90^o]$, of the transmitter with respect to the receiver are evaluated. This rotation is supposed to represent the roll of the aircraft.

The RSSI is also measured when there is a horizontal rotation of the transmitter in the inertial frame, which represents both differences in heading and the angle between the UAVs when they are not traveling in parallel. This angle is donated as ϑ and the result is further discussed in Chapter 12. This rotation is not performed by a servo motor; instead, the module is displaced manually for steps of 30^o.

The distances are measured manually and 50 groups of signal strength data $(d, RSSI, \phi, \vartheta)$ are collected in each position. Measurements were taken at increasing distances until the receiver was not able to read the majority of the packets. These packet losses occurred due to the receiver sensitivity, see Section 6.2.

To remove outliers of the RSSI signal, a Kalman filter is applied at each combination of d, $RSSI$, ϕ, and ϑ. In order to estimate the signal attenuation coefficient η, the mean of the state estimate from the Kalman Filter at each position is compared to the theoretical RSSI value in (7.1). The sample variance of the RSSI is calculated in each node to see how the noise X_σ affects the distance estimation error.

10.2 Transmitter Variations

In order to quantify the variability among different transmitter-receiver pairs, an attempt of comparing the two communication modules was made. The transmitter was used as a receiver and vice versa, while measurements were taken at several distances (only for $\phi = 0$ and $\vartheta = 0$) in order to see if the radiation pattern and signal strength were equal for both modules.

11

Simulations

The simulations are implemented in a 2-D environment in MATLAB. The designated area of interest is decomposed into a set of grid cells. All UAVs maintain a grid-based belief map and initially, all cells have equal probability of containing a victim. The cells are initialized with a value of 0.5, which represents the probability of the presence of a victim. The attractive potential to the cell is first computed based on distance and angle from the UAV and then multiplied by the cell value. When a cell has been scanned and no victim is detected, the cell value is set to zero. The cells are assumed to be uncorrelated and the belief map is only updated for the cells in which the observation occurs.

Each UAV can detect, within a circular region centered on itself, if the nearby terrain cells have been covered by itself or by other UAVs.

A cluster of UAVs is randomly deployed somewhere in the search area. Multiple static targets are located within the area of interest. For stationary randomly positioned targets, the mission could be defined equally as a target search mission or as an area coverage mission. The following is a list of the functionality and assumptions designed into the simulator:

- The environment is defined as a quadratic region of size 3.5x3.5 km. The area is subdivided into a grid of cells in order to compute potentials and to determine coverage. Each cell is 20x20 meters, but this size is easily adjustable if desired.

- Virtual obstacles are positioned at the border of the area of interest to prevent agents getting out of bounds.

- Each UAV is able to fly at a varying speed within an adjustable interval, see Chapter 8. The desired speed is computed through the potential functions described in Chapter 4. Control dynamics of the speed is bounded by the speed interval and the maximum acceleration and deceleration. The minimum and maximum velocity is 20 m/s and 30 m/s, respectively. The maximum acceleration and deceleration are both set to 10 m/s^2.

- The turning rate is limited by the bank angle and turning radius, see Chapter 8 for details.
- Each UAV is equipped with various sensors:
  - One circular ground sensor with adjustable radius to detect possible targets. In the simulations, the UAVs operate at a constant altitude, where the camera covers a circular area with a radius of 80 m.
  - Wireless RF communication modules for distance measurements and position estimation.
- Obstacles are static and randomly distributed throughout the region.
- All victims are considered to be static. The cameras can recognize victims and the UAVs report to the base station if something is detected.

It is possible to modify the size of the area of interest, the number of UAVs and victims, the camera and communication range, etc.

The simulation time of scanning an area of 3.5x3.5 km is approximately 20 minutes for a swarm size of 15 UAVs.

11.1 Discrete Dynamic Model

The equations below use the states from the dynamic model described in Section 8.2. In this section, the EKF presented in (9.3)-(9.10) is developed for this particular simulation and the initial matrices are evaluated. The initial errors are assumed to be uncorrelated, which results in a diagonal **P** matrix. The model is discretized with a sampling time T_s of 0.2 seconds. The prediction steps are expressed in (11.1)-(11.2).

$$\hat{\mathbf{x}}_{k+1|k} = \mathbf{f}(\hat{\mathbf{x}}_k, 0, 0) = \begin{pmatrix} \hat{x}_k + T_s \hat{V}_k \cos \hat{\psi}_k \\ \hat{y}_k + T_s \hat{V}_k \sin \hat{\psi}_k \\ \hat{V}_k \\ \hat{\psi}_k \end{pmatrix} \tag{11.1}$$

$$\mathbf{P}_{k+1|k} = \Phi_k \mathbf{P}_{k|k} \Phi_k^T + \Gamma_k \mathbf{Q}_k \Gamma_k^T \tag{11.2}$$

$$\Phi_k = \frac{\partial \mathbf{f}(\hat{\mathbf{x}}_k, 0, 0)}{\partial \mathbf{x}_k} = \begin{pmatrix} 1 & 0 & T_s \cos \hat{\psi}_k & -T_s \hat{V}_k \sin \hat{\psi}_k \\ 0 & 1 & T_s \sin \hat{\psi}_k & T_s \hat{V}_k \cos \hat{\psi}_k \\ 0 & 0 & 1 & 0 \\ 0 & 0 & 0 & 1 \end{pmatrix} \tag{11.3}$$

$$\Gamma_k = \frac{\partial \mathbf{f}(\hat{\mathbf{x}}_k, 0, \hat{\mathbf{w}}_k)}{\partial \mathbf{w}_k} = \begin{pmatrix} 0 & 0 \\ 0 & 0 \\ 1 & 0 \\ 0 & 1 \end{pmatrix} \tag{11.4}$$

$$\mathbf{Q}_k = \begin{pmatrix} w_v & 0 \\ 0 & w_\psi \end{pmatrix} \tag{11.5}$$

Q is the covariance matrix of the process noise, i.e how often UAVs change direction and how erratically they move. These values depend on the current speed and heading angle, as well as the maximum turning rate and maximum acceleration and deceleration. The process noise decreases for higher sample rates. The measurement update is given below.

$$\mathbf{H}_{k+1} = \frac{\partial \mathbf{h}_{k+1}(\hat{\mathbf{x}}_{k+1|k}, 0)}{\partial \mathbf{x}_{k+1}} = \begin{pmatrix} 1 & 0 & 0 & 0 \\ 0 & 1 & 0 & 0 \end{pmatrix} \tag{11.6}$$

$$\mathbf{K}_{k+1} = \mathbf{P}_{k+1|k}\mathbf{H}_{k+1}^T(\mathbf{H}_{k+1}\mathbf{P}_{k+1|k}\mathbf{H}_{k+1}^T + \mathbf{R}_{k+1})^{-1} \tag{11.7}$$

$$\hat{\mathbf{x}}_{k+1|k+1} = \hat{\mathbf{x}}_{k+1|k} + \mathbf{K}_{k+1}(\mathbf{y}_{k+1} - \mathbf{h}_{k+1}(\hat{\mathbf{x}}_{k+1|k}, 0)) \tag{11.8}$$

$$\mathbf{P}_{k+1|k+1} = (\mathbf{I} - \mathbf{K}_{k+1}\mathbf{H}_{k+1})\mathbf{P}_{k+1|k} \tag{11.9}$$

In the experiments of the thesis, the measurement noise are assumed to be uncorrelated and the diagonal values of the **R** matrix are based on sensor noise variances. The initial measurement noise matrix is set according to GPS accuracy and both the x and y coordinates are assumed to be provided with an accuracy of 5 meters, i.e. $\mathbf{R}_0 = diag(5^2, 5^2)$. The Kalman filter is more aggressive and active at higher frequencies if the diagonal elements in **Q** are large compared to the elements in **R**.

If the guess of the initial states is too far from the true values, the positioning will never achieve accurate results. The position errors will follow through the entire simulation since there is no way to re-calibrate the position without GPS signals or access points with known positions.

11.2 Flow Chart

The flow chart in Figure 11.1 represents the decision-making for each UAV at each time step. This is used in the first development of the swarm behavior when the true positions are assumed to be known.

1. Check the distance from the UAV to unvisited cells and calculate the attractive potential as a function of distance and angle separation between the yaw angle and the angle to the cell. The potential is greater for shorter distances and smaller angle differences.

2. Measure the distance from the UAV to obstacles and boundaries and calculate the repulsive potential as a function of distance and angle separation between the yaw angle and the obstacle. The potential is greater for shorter distances and smaller angle differences.

3. Compute the distance from the UAV to all the other UAVs within communication range. Calculate the repulsive and attractive potentials as functions of distance and difference in yaw angle between agents. U_{rep} is inversely proportional to yaw differences while U_{atr} is proportional. For robustness, both potentials also depend on the number of UAVs within their communication range.
4. Compute the desired speed as a sum of all potentials. The potential functions are all vectors originating from neighboring UAVs, obstacles, and unvisited cells. The desired speed is used as a reference and is bounded by the minimum and maximum speed and acceleration limit, see Chapter 8 for details.
5. Compute the desired yaw angle from the potentials the UAV is exposed to. The desired yaw angle is evaluated from the sum of all potentials. Verify that the desired yaw subtracted by the current yaw does not exceed the maximum turning rate multiplied by T_s.
6. Update position, speed, and yaw angle by applying Equation (8.10) from Section 8.2.

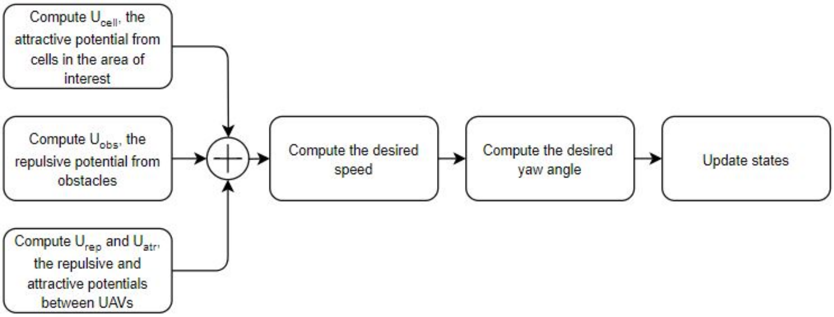

Figure 11.1 Flow chart of MATLAB simulations for UAVs with known position.

The computational time of calculating the potential functions and the desired speed and yaw angle must not exceed the sampling time T_s. This problem did not arise in the simulations.

For the swarm with estimated positions, the same steps are performed. However, before the potential functions are evaluated, the position of the UAV is estimated, see Figure 11.2. First, the position is estimated by minimizing the WNLS cost function of the distance measurements from nearby agents. Thereafter, an extended Kalman filter is applied, to account for aircraft dynamics. When the position estimate is combined with the dynamic motion model, false positions will generally be eliminated. The WNLS in the multilateration approach described in Section 7.3

may provide incorrect results due to numerical errors, or present two solutions. The latter occurs when only two UAVs are within communication range. If the signal path is obstructed, e.g. by a bird, the RSSI will contain less power due to reflections and/or absorption. If the estimated position is far from the previous position and does not follow the motion model, the most recent RSSI value is disregarded and dead reckoning is applied, see (11.10). These occurrences are added to the simulations randomly.

$$\begin{aligned} x_{k+1} &= x_k + T_s V_k \cos \psi_k \\ y_{k+1} &= y_k + T_s V_k \sin \psi_k \end{aligned} \tag{11.10}$$

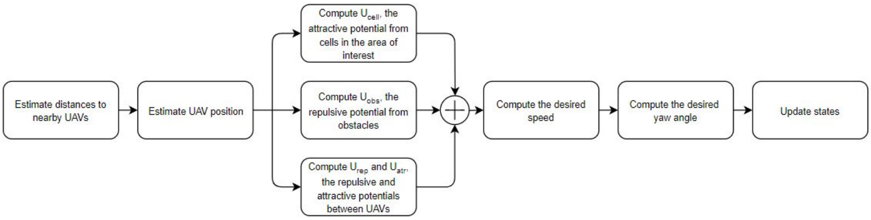

Figure 11.2 Flow chart of MATLAB simulations for UAVs with estimated position.

For the simulation with estimated UAV positions, the first two steps of the numbered list on page 62 are not affected. However, for the third step, the distance is estimated according to (12.2) and Table 12.1. Since there are no RSSI measurements available in the simulations, noise and biases are added to the true distance, according to the evaluated model. Thereafter, the potentials are calculated from this distance estimate. In step 4 and 5, the desired speed and yaw angle will differ from the previous simulation, since these are computed from the potential fields, which are position dependent.

The swarm members only communicate with the neighbors in LOS, and if there is an obstacle between an agent-pair, the code is written such that the UAVs on each side of the obstacle cannot detect each other. Obstructions of the signal path will result in an attenuation of the signal power. Even though a fraction of the signal might pass through the obstacle, the power will most likely not be strong enough for the receiver to detect.

12

Results

The results from the measurements and simulations are presented in this chapter. First, the static data of the RSSI measurements at different distances and angles are presented, and from this, a distance model is evaluated. Further, the swarm behavior is presented when the UAV positions are known. Lastly, the result from the distance estimate model combined with the developed swarm algorithm is presented.

12.1 Distance Estimate Model

The transmitter power at 1 m is measured to be -54 dBm. Figure 12.1 shows the RSSI values at four different distances and the effect of a Kalman filter on raw RSSI data. The measurements are taken by static devices (i.e. no movement of the receiver or transmitter) and when both ϕ and ϑ are zero. Note that the RSSI is represented as an integer and due to the poor accuracy, the signal strength often fluctuates between two values.

When comparing the modules, both devices transmitted a power of -54 dBm at one meter and no major differences between them were detected. However, a model evaluation for each sensor before deployment should be considered.

Antenna Characteristics

Two wire antennas were used in the experiments and according to the theory, their radiation pattern should be omnidirectional. When studying the signal propagation in a plane perpendicular to the direction of the antenna, the pattern should obtain the shape of a circle. Figure 12.2 shows the vertical and horizontal RSSI at 100 m, and as expected, the radiation pattern shows properties of an omnidirectional antenna. At this particular distance, the receiver could not handle data packages for $-80^o > \phi > 60^o$, due to the limited receiver sensitivity.

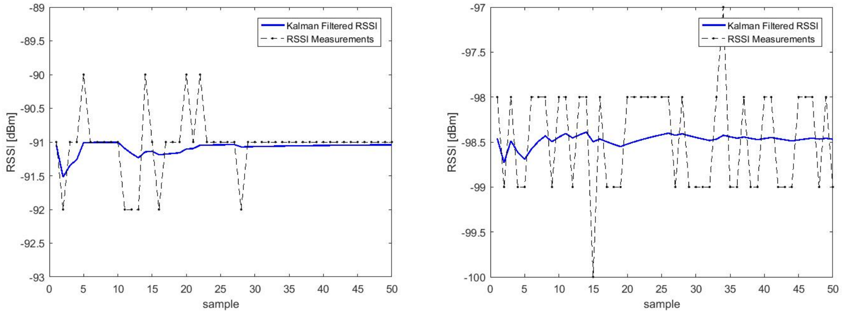

(a) RSSI at 50 m

(b) RSSI at 100 m

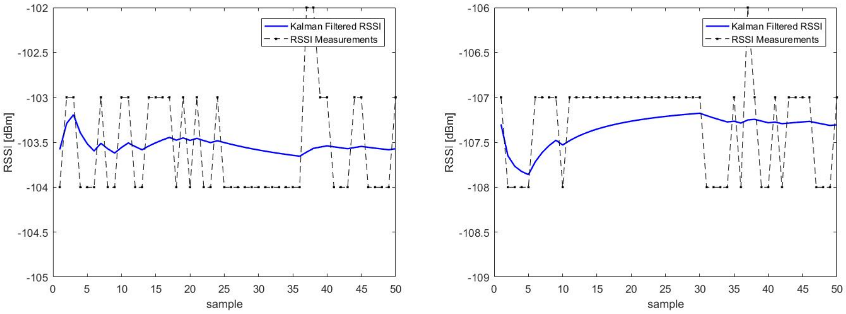

(c) RSSI at 150 m

(d) RSSI at 200 m

Figure 12.1 RSSI measurement values at static distances with a transmitting angle of zero with respect to the receiver. The black dots represent each sample of the RSSI measurements, and the thick blue line is the filtered RSSI estimate. The communication modules measure the signal strength as an integer number, which explains the RSSI fluctuation.

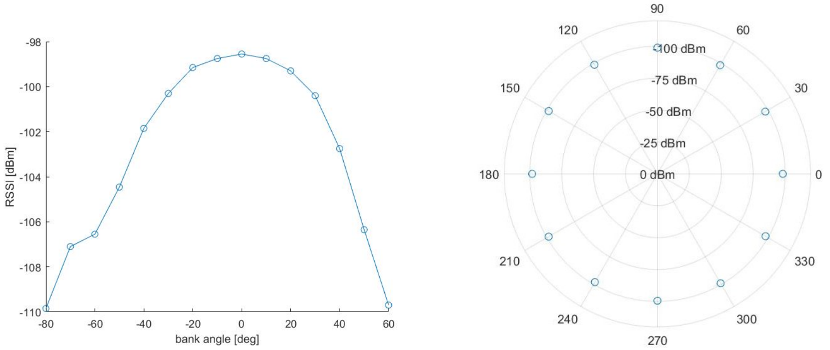

(a) Horizontal plane pattern

(b) Polar plot of the vertical plane pattern

Figure 12.2 Radiation pattern of the wire antennas used for taking measurements, at a distance of 100 m

The experiments show that the antenna orientation has a great impact on the RSSI values. If there is a height difference or nonzero bank angle between the transmitter and the receiver, the antenna orientation becomes a major factor that greatly affects the signal propagation model. Differences in height of the communication devices produce very unpredictable RSSI values and an attempt to infer distance information directly from the RSSI values is impossible.

Quadruple Slope Model

From the log-normal shadowing model in (7.1), η changes depending on the received signal strength, see Figure 12.3. Different techniques can be applied in order to achieve a suitable model for the RSSI-distance relationship. For the RSSI measurements in Figure 12.3, a double slope model will not achieve satisfactory results since the signal attenuation coefficient seems to obtain four different values. Instead, a quadruple slope model is applied for the following combinations of η and RSSI values for distances from 1 to 230 meters.

$$\eta = \begin{cases} 2.00 & \text{if} \quad -54 > RSSI \geq -82 \\ 2.18 & \text{if} \quad -82 > RSSI \geq -99 \\ 2.28 & \text{if} \quad -99 > RSSI \geq -106 \\ 2.32 & \text{if} \quad -106 > RSSI \end{cases} \tag{12.1}$$

For this particular model, three distance gaps for RSSI values of -82, -99, and -106 dBm will occur. The gap at -82 dBm does not yield a problem since the UAVs do not operate at this distance from each other. However, the other two gaps will result in significant model errors. Another RSSI based approach is the $\alpha\beta$-model, which eliminates this problem.

$\alpha\beta$-Model

The $\alpha\beta$-model is expressed in (10.2), where the parameters have been tuned for a minimum sum of residuals in the distance interval 100-200 m since those are the general distances kept between agents. This model yields bias offsets for short distances around 5-25 m, but this error is neglected due to the fact that the agents never fly this close to each other.

$$P(d) = P(d_0) - 10 \cdot 2.15 \log_{10}\left(\frac{d}{d_0}\right) - \frac{d^{1.3}}{250} + X_\sigma \tag{12.2}$$

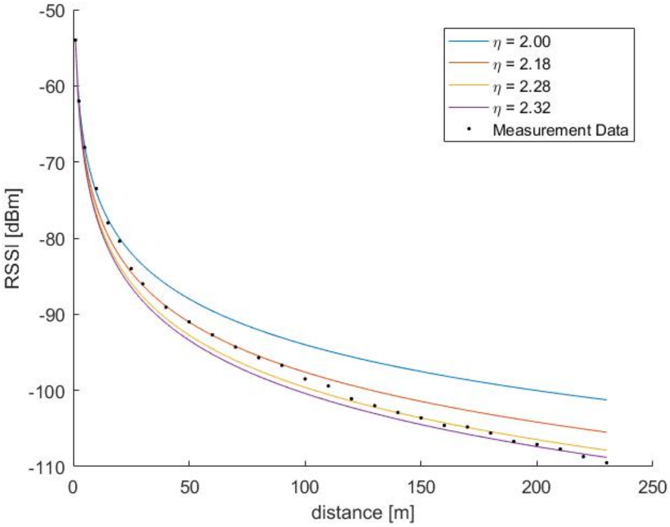

Figure 12.3 RSSI as a function of distance. The solid lines represent the theoretical relationship from (7.1), with varied η. The black dots represent the experimental RSSI values (mean of KF estimates) at measured distances. The transmitting angle is zero with respect to the receiver.

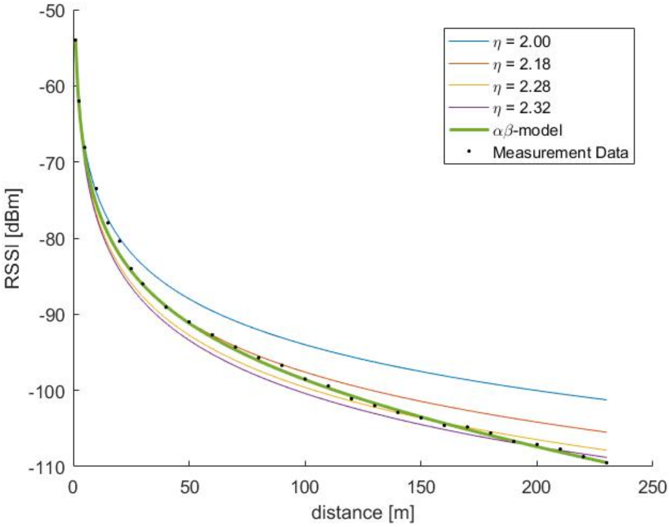

Figure 12.4 RSSI as a function of distance. The thin solid lines represent the theoretical relationship from (7.1), with varied η. The green thick line represents the $\alpha\beta$-model where $\eta = 2.15$, $\alpha = 1/250$ and $\beta = 1.3$. The black dots represent the experimental RSSI values at measured distances. The transmitting angle is zero with respect to the receiver.

RSSI	$\hat{d}$
-95	72.2
-96	79.2
-97	86.8
-98	94.9
-99	103.6
-100	112.9
-101	122.8
-102	133.3
-103	144.4
-104	156.1
-105	168.4
-106	181.2
-107	194.6
-108	208.5
-109	223.0
-110	237.8

Table 12.1 RSSI values and their corresponding distance estimates. The RSSI is in dBm and the distance is in meters. The transmitting angle is zero with respect to the receiver.

If the $\alpha\beta$-model is applied, the noise is estimated through the measurements. In order to estimate the pdf of the noise, several measurements are taken. White noise is assumed and the pdf is evaluated from the model as $X \sim \mathcal{N}(0, 0.61)$.

The RSSI values and their corresponding distance estimates when ϕ and ϑ are zero can be seen in Table 12.1.

As seen in the table, the distance error increases with a decreased signal strength. Since the RSSI value is represented as an integer, the positioning does not yield very accurate results. Compare these values to Figure 12.2 where for a distance of 100 m, the RSSI fluctuates between -98 and -99 dBm. According to the model, these values represent distances of 94.9 and 103.6 m. If outliers occur as a result of disturbances, the RSSI value could reach -97 or -100 dBm, which represent distances of 86.7 and 112.9 m, respectively. This would correspond to distance errors of around 13 meters.

However, since the UAVs generally keep a distance of 120 m to the neighboring agents, a position error of 10-15 m will generally not result in collisions between agents. Position errors can however cause the agents to believe they have scanned areas they have not yet visited.

Transmitter Rotation

The bank angle is represented by an automatic rotation of the transmitter from -90^o to 90^o in increments of 10^o. For each distance and bank angle, the transmitter is manually rotated about the horizontal plane of an inertial coordinate frame parallel to the Earth. As mentioned in Chapter 10, not only does the RSSI depend on the distance and the difference in roll and yaw, but also on the position relative to another aircraft, see Figure 12.5.

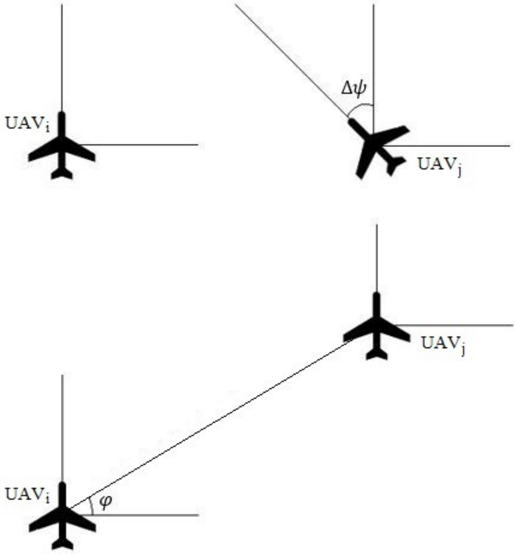

Figure 12.5 Illustration of heading angle difference $\Delta\psi$ and angle between agents φ as reference for the RSSI-distance model.

The receiver sensitivity of the communication modules is -110 dBm, and a majority of the signals when the absolute value of ϑ was less than 30^o and the absolute value of the bank angle exceeded 40^o were not received for distances above 100 meters. When the RSSI values were close to -110 dB, multiple package losses occurred, which makes the signal power unreliable. In other words, if the difference in bank between an agent pair exceeds a certain value for large distances, no RSSI value can be detected. One way to account for this is to limit the bank angle by a maximum value. Another way is to neglect the RSSI values in the position estimation algorithm when the difference in bank between the receiver and the transmitter exceeds a certain value. For these cases, dead reckoning can be applied.

50 measurements were taken at each combination of position and orientation. In Figure 12.6, the mean values for distances of 100, 150, and 200 meters are plotted.

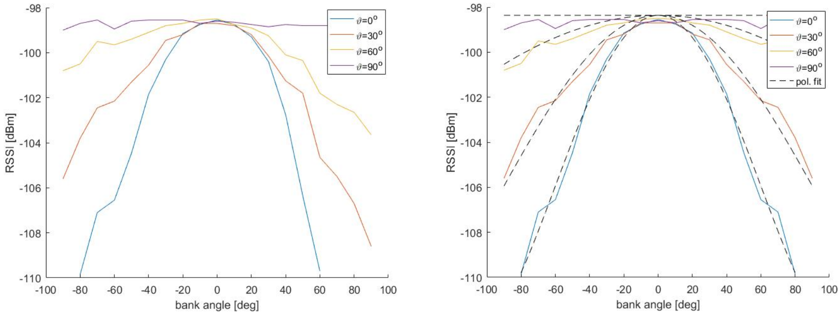

(a) RSSI at 100 m (b) RSSI at 100 m, mirrored in *y* axis

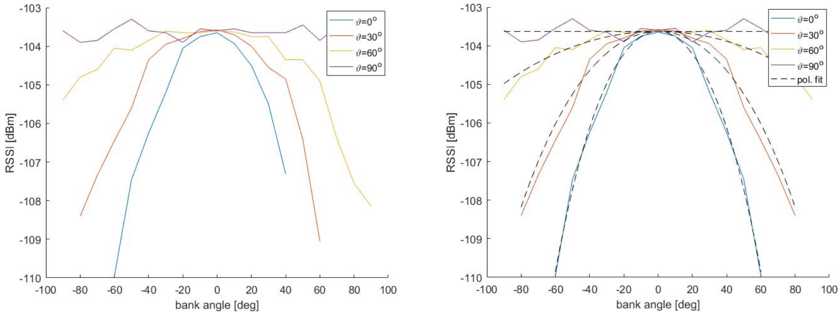

(c) RSSI at 150 m (d) RSSI at 150 m, mirrored in *y* axis

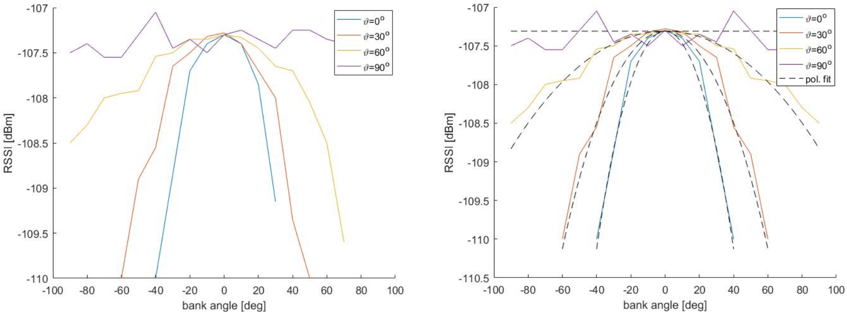

(e) RSSI at 200 m (f) RSSI at 200 m, mirrored in *y* axis

Figure 12.6 RSSI values at static distances and varying angles. The mirrored plots in the right column represent the results if each agent is assumed to be equipped with two communication devices. The same polynomial fit is used for all distances, see (12.3).

The shape of the RSSI as a function of bank angle corresponds to the omnidirectional pattern expected for wire antennas. In order to find an accurate model for this relationship, a polynomial fit is applied to the measurement data. The computational complexity grows with the order of the polynomial, but to eliminate large errors, a fifth order polynomial for RSSI versus bank is chosen. For lower orders of polynomials, the modeled RSSI values around a zero degree bank are significantly lower than the measured RSSI. Figure 12.7 illustrates the 3-D polynomial fit at a distance of 100 m. By comparing the data from all distances, a model between the estimated distance as a function of heading, bank, and RSSI is evaluated.

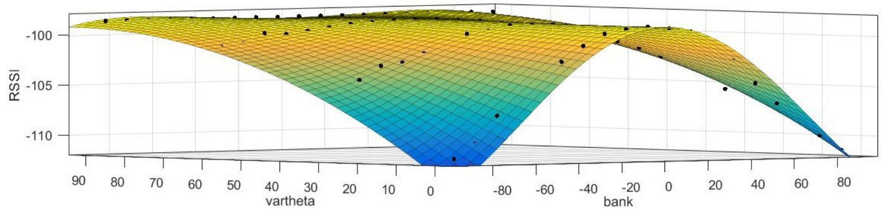

Figure 12.7 Polynomial fit of RSSI values versus ϑ and bank angle ϕ at a distance of 100 m.

Equation (12.3) represents the 2-D polynomial illustrated in Figure 12.5 (b), (d), and (f). In (12.4), the yaw angle dependency is also taken into account.

$$\begin{aligned} P(0,\phi,d) = P(0,0,d_0) - 10\eta\log_{10}\left(\frac{d}{d_0}\right) - \alpha d^{\beta} + \\ X_{\sigma} + a\phi^4 + b|\phi|^3 + c\phi^2 + e|\phi| \end{aligned} \tag{12.3}$$

$$\begin{aligned} P(\psi,\phi,d) = P(0,0,d_0) - 10\eta\log_{10}\left(\frac{d}{d_0}\right) - \alpha d^{\beta} + X_{\sigma} + a\left(\phi\left(1-\frac{2\vartheta}{\pi}\right)\right)^4 + \\ b\left|\phi\left(1-\frac{2\vartheta}{\pi}\right)\right|^3 + c\left(\phi\left(1-\frac{2\vartheta}{\pi}\right)\right)^2 + e\left|\phi\left(1-\frac{2\vartheta}{\pi}\right)\right| \end{aligned} \tag{12.4}$$

ϑ is the absolute value of the difference in yaw angle, ψ, minus the angle between the two aircraft with respect to the global x axis. See Figure 12.5 for an illustration.

$$\vartheta = |\Delta\psi - \varphi| \tag{12.5}$$

12.2 Simulations of UAVs with Known Positions

When a swarm of 15 UAVs is simulated by rules of potential fields, the result for the first 600 time steps ($T_s = 0.2$ s) is shown in Figure 12.8 and 12.9. The starting position is in the bottom left corner and the initial positions and the heading angles are equal in both simulations. In Figure 12.8, no obstacles are present, while two static obstacles are in the path of the swarm in Figure 12.9 during this time span. When the simulation starts, most of the distances between the UAVs are shorter than optimal. When the UAVs are exposed to potential fields when initially finding their optimal relative position, small oscillations occur. It takes longer for the UAVs to settle and find their optimal relative position in the swarm when there are obstacles present, a behavior that is expected.

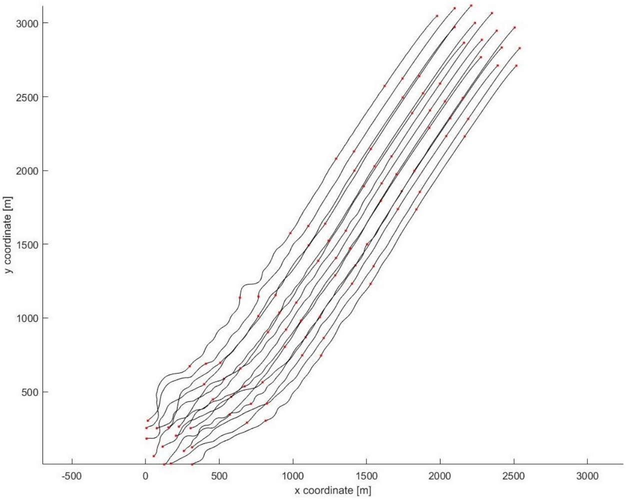

Figure 12.8 Simulation of a swarm of 15 UAVs for the first 600 time steps (flight time of 120 seconds), when no obstacles are present. The starting position is in the bottom left corner and the red dots represent the UAVs position at each 100^{th} time step. Each UAV path is illustrated as a black line.

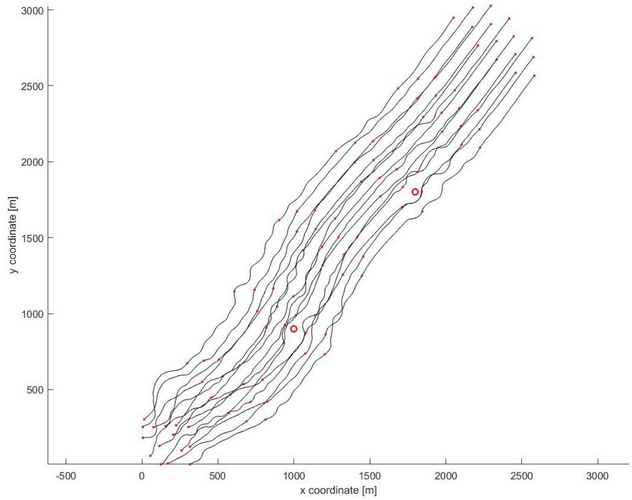

Figure 12.9 Simulation of a swarm of 15 UAVs for the first 600 time steps (flight time of 120 seconds), when obstacles are present. The starting position is in the bottom left corner and the red dots represent the UAVs position at each 100^{th} time step. Each UAV path is illustrated as a black line. Static obstacles are represented as red circles. No collisions occur between neither agent pairs nor agents and obstacles.

For an area of 3500x3500 m, it takes approximately 4500 time steps (15 minutes) for the UAVs to scan 90 % of the area. For faster coverage, the UAVs could travel in a formation, such as a line or in a *V* shape like birds. However, since their communication range is limited, disconnections in the swarm may occur if one UAV loses connection or is subject to some technical failure. The system is more robust to failures if the agents are traveling in a cluster. When traveling in a cluster, the UAVs are able to handle the loss of members. Individual failures, such as hardware or software failures that result in a broken airplane, will generally not lead to communication losses within the swarm.

Four different initial setups were used in the simulations as it ran for 4750 time steps. The percentage of scanned cells were evaluated for each setup, see Figure 12.10 and Table 12.2.

	Setup 1	**Setup 2**	**Setup 3**	**Setup 4**
Covered Cells	96.6 %	96.2 %	92.5 %	91.6%

Table 12.2 Percentage of covered cells for four different initial setups. The flight time was set to 950 seconds (4750 time steps).

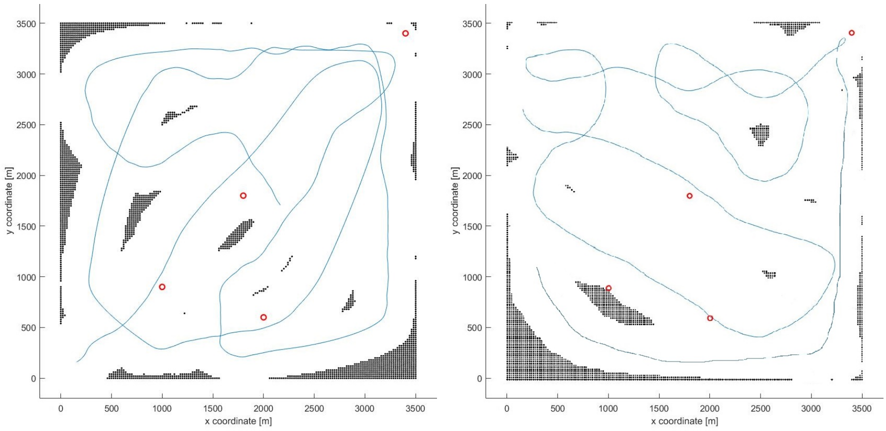

(a) Starting positions at appx. $(x, y, \psi) = (100, 100, \pi/4)$

(b) Starting positions at appx. $(x, y, \psi) = (200, 2600, -\pi/4)$

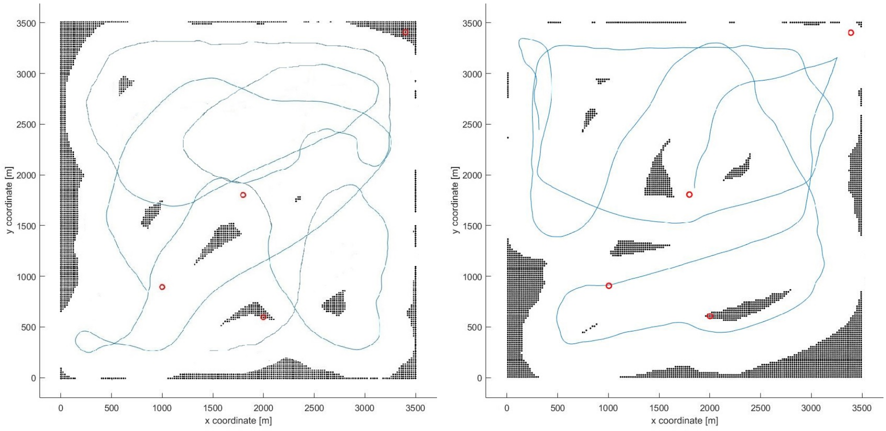

(c) Starting positions at appx. $(x, y, \psi) = (800, 800, 2\pi/3)$

(d) Starting positions at appx. $(x, y, \psi) = (1800, 1800, 4\pi/9)$

Figure 12.10 Path of the swarm for four different initial positions, represented as a mean value of all UAV positions at all time steps. The red circles are stationary obstacles and the black dots represent the remaining unscanned cells after a simulation of 4750 time steps. The swarm covers above 90% of the area for all setups, and most areas are not scanned multiple times.

The result in Figure 12.10 and Table 12.2 is affected by the placements of the obstacles, but in general, the starting positions will not affect the behavior of the swarm, as long as all of the members are placed within communication range to each other. For the developed algorithm, the UAVs generally keep a minimum distance of approximately 30 meters to the obstacles and all collisions are successfully prevented. As described in Chapter 11, the UAVs generally cannot communicate if there is an obstacle present between them. If an obstacle is too big or if a group of obstacles obstruct the path of the swarm, the UAVs will most likely split up into multiple subsystems, as explained in Chapter 4. This case was simulated, see results in Figure 12.11, where the red circle represents an obstacle and the red dots are the UAV positions every 100^{th} time step. The UAVs' initial positions are in the bottom left corner (setup 1).

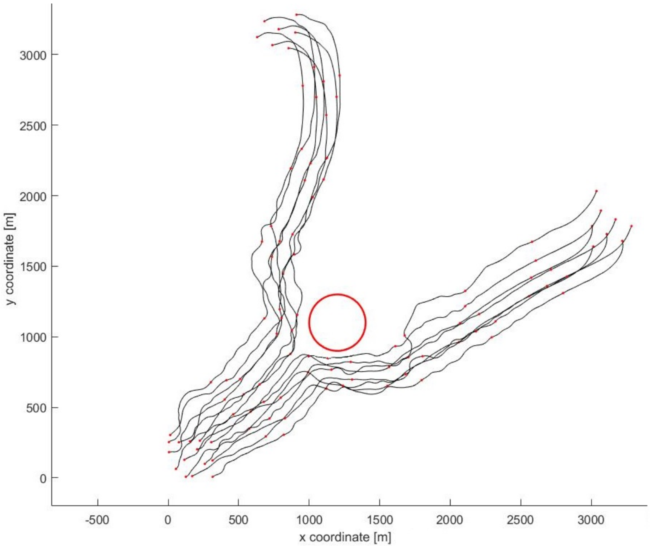

Figure 12.11 Simulation of a swarm with a large stationary obstacle present. The initial positions are in the bottom left corner and the red dots represent the UAVs' positions at each hundredth time step. Each UAV path is illustrated as a black line. A large static obstacle is represented as a red circle. No collisions occur between agent pairs or agents and obstacles. However, the swarm split up into two swarms when preventing the obstacle collision.

The UAVs keep a distance of approximately 120 meters to their closest neighbor. A plot of this for setup 1 is illustrated in Figure 12.12. As seen in the figure, the closest distance to a neighboring UAV is approximately 50 meters and the longest is around 170 meters. With this said, they never collide with each other or lose communication since the distance does not exceed the communication range.

By studying the fluctuations and distance variations at certain time instants in Figure 12.12, it can be shown that these distance variations generally occur when the UAVs approach corners, borders, and obstacles.

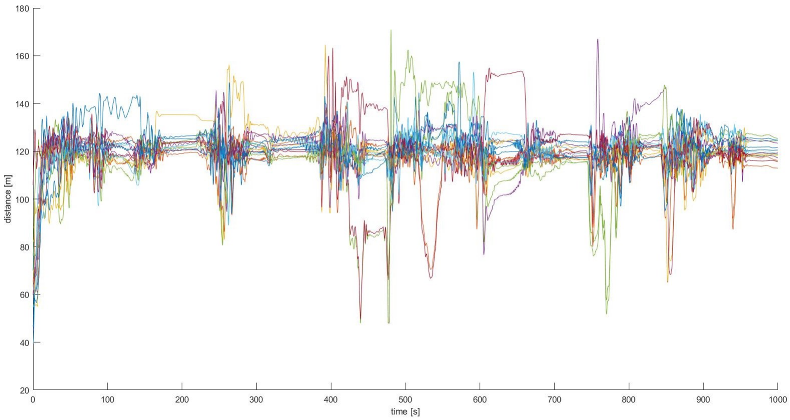

Figure 12.12 Distance to closest neighbor for all 15 UAVs for 1000 seconds.

12.3 Simulations of UAVs with Estimated Positions

To use estimated positions throughout the simulations, the initial positions of the UAVs must be provided. This can be achieved by assuming multiple access points with known positions on the ground. The APs broadcast their own position in order for the UAVs to estimate their position by multilateration. In the simulations, the UAVs are assumed to be provided their true initial position with an accuracy of $\pm$ 5 m. Random initial positions are chosen (no risk of collisions at the start) and random uniform noise with standard deviation 5 is added.

Throughout the simulation, the position offset between the true position and the estimated position was around 9 m in average. In Figure 12.13, the position estimation error for all UAVs are included in a histogram, for a simulated flight time of 1000 seconds. For this particular simulation, a normal distribution is estimated from the histogram values, with the mean value $\mu = 8.90407$ m and a 95% confidence interval of [8.89252, 8.91562] m. The standard deviation is $\sigma = 1.61384$ m with a 95% confidence interval of [1.60535, 1.62168] m. The position estimation was performed for several initial setups, and the mean offset was approximately 8.9 meters for most simulations.

Occasionally, the WNLS method provides false positions due to numerical errors, but these are filtered out by the EKF. When there is an obstacle along the path of the swarm, one UAV might only have two other members within its communication range. When this occurs, dead reckoning is used to estimate the UAV's position.

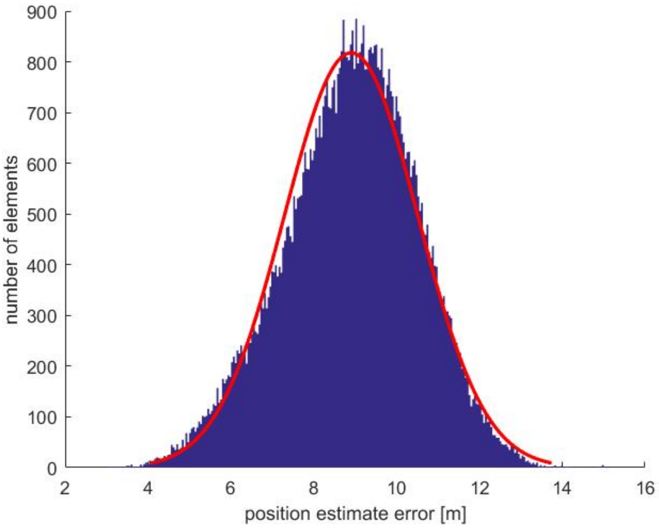

Figure 12.13 Position offset between the true and estimated position of all 15 UAVs. The red line represent a normal distribution with mean value $\mu \approx 8.9$ m and standard deviation $\sigma \approx 1.6$ m.

For this approach, no collisions occur between agent pairs, or agents and obstacles. Neither do the UAVs go out of bounds. A plot of the distance to the closest member is seen in Figure 12.14. At a few time instances, one UAV has the closest neighbor at a distance of 200 m and the shortest at a distance around 23 m. This result can be compared to the result in Figure 12.12. In the simulation of estimated positions, more oscillations occur due to noise and uncertainties of the RSSI measurements.

For the simulation with estimated positions, the number of scanned cells for 4750 time steps is approximately equal to the number in the simulations with known positions. The swarm takes a different path when the positions are estimated, but no significant difference was found regarding the efficiency of scanning the area. However, due to the position error, the swarm covers certain cells twice in one simulation while missing neighboring cells. If the UAVs believe they have visited certain areas they have not yet scanned, victims may go undetected. Random noise is added to the estimated positions, for the same four different setups as for the simulation with known positions. The result varied from each repetition of the same simulation, and a table corresponding to Table 12.2 is not created for these cases. Approximately the same number of cells were covered for all four different setups.

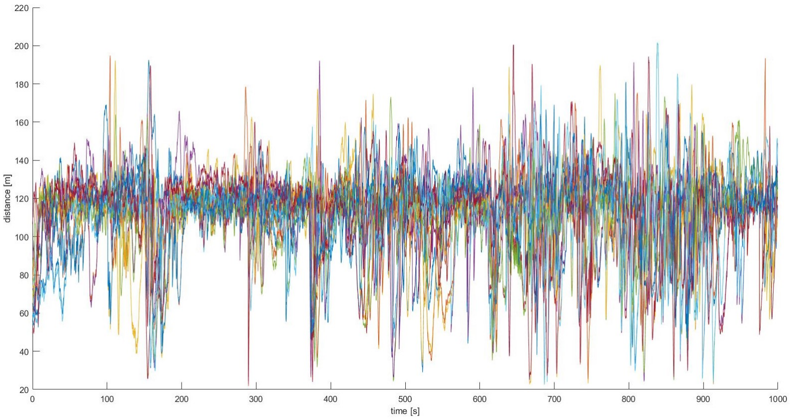

Figure 12.14 Distance to closest neighbor for all 15 UAVs for 1000 seconds, when the positions are estimated.

13

Conclusion

In this chapter, the contributions made throughout this thesis are presented. Further, possible extensions and improvements are described in the future work section. This chapter also covers the ethical aspects of the project.

13.1 Contribution

In previous research using RSSI for position estimation, the LNSM-model has been extended to the α-model. A contribution of this thesis was to add another parameter, β, which improved the model accuracy greatly.

The developed potential field algorithm did show promising results in terms of controlling the swarm when positions of the UAVs were considered to be known. The swarm behavior was studied throughout multiple initial setups, see Figure 12.10. The UAVs keep the formation of a cluster, and as seen in Figure 12.12, no collisions occur between agents.

The RSSI approach can only be used when UAVs are provided their starting position, since an error in their initial position can not be corrected for. However, the errors of the position estimates do not contribute to any risks of collision between neither agent pairs nor agents and obstacles. The former because a position error of 10 meters will not lead to collisions when the agents generally operate at a distance of 120 m to their closest neighbor. The latter because the UAVs measure the relative distance to obstacles by using sensors, such as radar. Their own global position and the position of the obstacle is not relevant.

However, due to position estimate errors, the agents might believe they have scanned certain areas they have not been to. If the UAVs are searching for victims, there is a risk they will go undetected.

Note that in the simulations, a 2-D environment is assumed and both the roll and the pitch angles are assumed to be zero. For real applications, this has to be accounted for.

13.2 Future Work

The primary focus on further developments should contain improvements of the signal quality and include disturbances. Disturbances may consist of different weather conditions and interference from other RF signals. The static measurements taken for the model evaluations can be improved by placing the communication devices on a tall ladder.

In order to test the developed approach on real aircraft, the kinematic motion model has to be extended to a 6 DoF model, used in a 3-D environment. To prevent collisions in 3-D applications, the UAVs also have the option to change altitude instead of just turning either left or right.

In the simulations, the UAVs were assumed to maintain a constant altitude and as mentioned in Chapter 11, if communication modules are not positioned at the same level, the radiation pattern will be affected. RSSI based position estimation is not accurate enough for high-speed maneuvers. The signal strength is highly dependent on the angle of transmission and large distance errors might occur if there is a time-lag of the received signal while a UAV performs a high-speed turn. RSSI based position estimation is not suitable for 3-D environments and an investigation of alternatives to RSSI measurements should be considered for these applications. One alternative is to use multilateration on WiFi signals from ground APs with known positions. When the transmitters are attached to the body of an aircraft, the propagation pattern is highly dependent on the bank angle, which makes the positions difficult to estimate, or sometimes even impossible. However, the RSSI-distance model evaluated in (12.4) does include non-zero bank angles. This may be used in further research, where ϑ (12.5) can be estimated by using the previous position of the UAVs involved, their acceleration, and yaw angles. When having no previous knowledge of the UAV position, it is impossible to estimate its position when the bank angle is non-zero.

The wire antenna may bend at high speed, which will result in a distorted radiation pattern. The RSSI based position estimation approach requires better antennae for real applications, e.g. a blade antenna.

Note that the simulation is a simplification of a real system. To use the potential field algorithm in real applications, time delays from signal packages should not be neglected. Each UAV may keep an individual map containing a time stamp of their most recent update. This should be shared between agents and updated when possible. In the simulations, the map is considered to be updated for all UAVs at the same time.

If there is a chance of non-stationary victims, the values of the scanned cells should increase over time. If an area has been searched once, the probability of finding a victim should not remain zero. Instead, the cell value should increase successively from 0 to 0.5 over time. Recently searched areas will result in smaller potentials and therefore be of less interest. This could be compared to the procedure of mowing a lawn, where the grass grows over time.

If the environment of where the UAVs perform their search algorithm is known beforehand, some areas might have a higher probability of containing a target. E.g. if a person disappeared in a river, the cell value should be set higher near the river and decline further from it. If no prior information is known, a uniform distribution is assumed.

All UAVs are assumed to be identical, but in real applications, wear of different components and small differences in sensor offsets may exist. As mentioned in Chapter 10, a model evaluation for each communication device should be considered before deployment.

For further developments, an optimization of the code may be considered. This has no relation to the performance of the algorithm, but improvements may reduce the computational costs and complexity of the program.

13.3 Ethical Aspects

When studying technology research and development, the ethical aspects should be considered. Many new technologies have come as a result of the military funding of science. Research and development of military products may be perceived as problematic, but at the same time, it creates a base for further development of a considerable amount of technology used for civilian applications. Military inventions have been brought into civilian use throughout history, with minor modification if any. Sensors and communication systems have been used to detect enemies and to coordinate movements of armed forces and automatic weapons. The technology of radar, laser guidance, and satellite guidance were all developed for military use. The GPS system was initially developed for use by the United States military, but today it plays an important role in our everyday lives.

Unmanned Vehicles

This particular Master's project uses civilian aircraft. However, the swarm algorithm developed in this thesis can be applied to military applications. UAVs scanning an area to find victims may equally be used to find people, classifying them as targets.

Unmanned aerial vehicles have been criticized a lot during recent years. However, UAVs can perform a broad range of applications within civilian use, where some of them are listed below.

- Detect and put out wildfires.
- Transport medicine and blood supplies to remote areas, or areas with washed out roads or downed phone lines.
- Transport defibrillators and other medical equipment much faster than an ambulance.
- Monitor wildlife and keep track of endangered species.

- Spot illegal hunting.
- Inspect oil rigs.
- Test air quality and the makeup of the ozone.
- Detect illegal waste dumping.
- Spy on farms in order to expose animal cruelty.
- Enter radiation-filled areas after nuclear accidents where human access would be dangerous.

UAVs may shorten the response times and at the same time reduce the risk for human rescue teams. Although UAVs may benefit search and rescue operations, technical advancements are needed to strengthen them against different risks, such as signal interference and threats. Threats include enemies, extreme weather conditions, bacteria, and toxic materials.

13.4 Conclusion

This paper addressed localization in outdoor environments for small, low-cost unmanned aerial vehicles. It has been shown that potential fields successfully can be applied to swarm algorithms of UAVs. The potential field algorithm developed in this thesis demonstrates that the UAV swarm completes the desired task, i.e. surveys an area collaboratively. This method can handle the loss of units and is potentially scalable to large, distributed networks of devices.

Existing localization techniques have been characterized and an RF-based localization method has been researched further. This method uses RSSI measurements in combination with a WNLS filter and multilateration techniques, by which each UAV estimates its position in a 2-D environment. This approach uses a simple signal propagation model but adapts to different environments in terms of size, shape, and number of obstacles. RSSI based position estimation is useful for a considerable amount of applications within civilian use with low accuracy requirements of the position. General problems have been outlined in the future work section, including adapting the localization method to noisy environments.

The result of the search algorithm for UAVs with known positions was compared to the simulations of estimated positions. No collisions occur between agent-pairs or agents and obstacles and the swarm stays within the search area for all simulations. However, the swarm takes a different path when the positions are estimated, but no significant difference was found regarding the efficiency of scanning the area. Due to the positioning error, the swarm covers certain cells twice in one simulation while missing neighboring cells. When this occur, victims may go undetected if the UAVs believe they have visited certain areas they have not yet scanned.

Bibliography

Ambrosino, G., M. Ariola, U. Ciniglio, F. Corraro, E. D. Lellis, and A. Pironti (2009). “Path generation and tracking in 3-d for uavs”. *IEEE Transactions on Control Systems Technology* **17**:4, pp. 980–988.

Atkins, E., A. Ollero, and A. Tsourdos (2016). *Unmanned Aircraft System*. 1st ed. John Wiley & Sons Ltd.

Baker, C., G. Ramchurn, L. Teacy, and N. Jennings (2016). “Planning search and rescue missions for uav teams”.

Bandala, A. A., E. P. Dadios, R. R. P. Vicerra, and L. A. G. Lim (2014). “Swarming algorithm for unmanned aerial vehicle (UAV) quadrotors - swarm behavior for aggregation, foraging, formation and tracking -”.

Beard, R. W. and T. W. McLain (2012). *Small Unmanned Aircraft, Theory and Practice*. Princeton University Press.

Bejiga, M. B., A. Zeggada, A. Nouffidj, and F. Melgani (2017). “A convolutional neural network approach for assisting avalanche search and rescue operations with UAV imagery”.

Beni, G. and J. Wang (1989). *Swarm intelligence in cellular robotic systems*. NATO Advanced Workshop on Robots and Biological Systems, Tuscany, Italy.

Blyenburgh, P. van (2010-2011). *UAS Yearbook - UAS: The Global Perspective*. 8th ed. Blyenburgh & Co.

Couzin, I. D., J. Krause, R. James, G. D. Ruxton, and N. R. Franks (2002). “Collective memory and spatial sorting in animal groups”. *J. theor. Biol.* **218**, pp. 1–11.

Deneubourg, J. and S. Goss (1989). “Collective patterns and decision-making”. *Ethology Ecology and Evolution* **1**, pp. 295–311.

Duan, H. and P. Qiao (2014). “Pigeon-inspired optimization: a new swarm intelligence optimizer for air robot path planning”. *International Journal of Intelligent Computing and Cybernetics* **7**:1, pp. 24–37.

Gaudiano, P., B. Shargel, E. Bonabeau, and B. T. Clough (2003). "Swarm intelligence:a new c2 paradigm with an application to the control of swarms of UAVs". *ICCRTS Command and Control Research and Technology Symposium* **8**.

Gazi, V., B. Fidan, S. Hanay, and M. I. Köksal (2007). "Aggregation, foraging, and formation control of swarms with non-holonomic agents using potential functions and sliding mode techniques". *Turk J Electrical Engineering* **15**:2, pp. 149–168.

Ge, S. and Y. Cui (2000). "Dynamic motion planning for mobile robots using potential field method."

Grimes, J. G. (2008). *Positioning System Standard Positioning Service Performance Standard*. 4th ed. Tech. rep. Department of Defense.

Gustafsson, F. (2012). *Statistical Sensor Fusion*. 2:1. Studentlitteratur.

Hexmoor, H., B. McLaughlan, and M. Baker (2005). "Swarm control in unmanned aerial vehicles". **2**.

Huang, Y.-J. and W. Zeng (2007). "A reliable routing protocol for multi-hop ad hoc networks". *Wireless Communications, Networking and Mobile Computing*.

Jaimes, A., S. Kota, and J. Gomez (2008). "An approach to surveillance an area using swarm of fixed wing and quad-rotor unmanned aerial vehicles UAV(s)". *System of Systems Engineering*, pp. 1–6.

Karlsson, F. and M. Karlsson (2014). *Sensor Fused Indoor Positioning Using Dual Band WiFi Signal Measurements*. Master's Thesis. Lund University.

Kennedy, J. (1995). "Particle swarm optimization". *IEEE International Conference on Neural Networks*, pp. 1942–1948.

Khatib, O. (1985). "Real-time obstacle avoidance for manipulators and mobile robots". *IEEE International Conference On Robotics and Automation, St. Loius Missouri*, p. 500505.

Kuipers, J. B. (1999). *Quaternions and Rotation Sequences*. Princeton University Press.

Kurdi, H. A., J. P. How, and G. Bautista (2016). "Bio-inspired algorithm for task allocation in multi-uav search and rescue missions".

Laboid, H., H. Afifi, and D. D. Santis (2007). *Wi-Fi, Bluetooth, ZigBee and Wimax*. 1st ed. Springer.

Lewis, M. A. and G. A. Bekey (1992). "Behavioral self-organization of nanorobots using local rules". *Conference on Intelligent Robots and Systems* **2**, pp. 1333–1338.

Luo, C., S. McClean, G. Parr, L. Teacy, and R. D. Nardi (2013). "UAV position estimation and collision avoidance using the extended kalman filter".

Mai, T. (2012). *Global positioning system history*. `https://www.nasa.gov/directorates/heo/scan/communications/policy/GPS_History.html`.

Mautz, R (2012). *Indoor Positioning Technologies*. Habilitation thesis. ETH Zürich.

NSF, N. S. F. (2005). *Small, unmanned aircraft search for survivors in katrina wreckage*. `http://www.nsf.gov/news/news_summ.jsp?cntn_id=104453&org=EEC`.

Partridge, B. L. (1982). "Structure and function of fish schools". *Scientific American* **246**:6, p. 114.

Qi, J., D. Song, H. Shang, N. Wang, C. Hua, C. Wu, X. Qi, and J. Han (2015). "Search and rescue rotary-wing UAV and its application to the lushan ms 7.0 earthquake".

Rappaport, T. (1996). *Wireless Communications - Principles and Practice*. IEEE Press.

Reynolds, C. W. (1987). "Flocks, herds and schools: a distributed behavioral model." *ACM SIGGRAPH Computer Graphics* **21**, pp. 25–34.

Ruan, D. (2010). *Computational Intelligence in Complex Decision Systems*. 1st ed. Atlantis Press.

Sauter, J. A., R. S. Matthews, J. S. Robinson, J. Moody, and S. P. Riddle (2009). "Swarming unmanned air and ground systems for surveillance and base protection".

Seybold, J. S. (2005). *Introduction to RF Propagation*. Wiley.

Shi, Y. and R. C. Eberhart (1998). "A modified particle swarm optimizer". *IEEE International Conference on Evolutionary Computation*, pp. 69–73.

Silvagni, M., A. Tonoli, E. Zenerino, and M. Chiaberge (2016). "Multipurpose UAV for search and rescue operations in mountain avalanche events".

Stickland, T. R., N. F. Britton, and N. R. Franks (1999). "Models of information flow in ant foraging: the benefits of both attractive and repulsive signals". *Information Processing in Social Insects*, pp. 83–84.

Trimble (2017). *All about GPS*. `http://www.trimble.com/gps_tutorial/whatgps.aspx`.

Varela, G., P. Caamamo, F. Orjales, A. Deibe, F. Lopez-Pena, and R. Duro (2011). "Swarm intelligence based approach for real time UAV team coordination in search operations". *Nature and Biologically Inspired Computing (NaBIC)* **3**, pp. 365–370.

Wen, X., W. Tao, C.-M. Own, and Z. Pan (2016). "On the dynamic RSS feedbacks of indoor fingerprinting databases for localization reliability improvement".

Yanmas, E., R. Kuschnig, and C. Bettstetter (2011). "Channel measurements over a 802.11a-based UAV-to-ground links". *Proc. IEEE GLOBECOM-WiUAV*.

Yokoyama, R. S., B. Y. L. Kimura, and E. dos Santos Moreira (2014). "An architecture for secure positioning in a uav swarm using RSSI-based distance estimation". *Applied Computing Review* **14**:2.

Lund University
Department of Automatic Control
Box 118
SE-221 00 Lund Sweden

Document name
MASTER’S THESIS

Date of issue
December 2017

Document Number
TFRT-6046

Author(s)
Märta Paulsson

Supervisor
Lars Pääjärvi, Saab AB
Magnus Blomberg, Saab AB
Bo Bernhardsson, Dept. of Automatic Control, Lund University, Sweden
Karl-Erik Årzén, Dept. of Automatic Control, Lund University, Sweden (examiner)

Title and subtitle
High-Level Control of UAV Swarms with RSSI Based Position Estimation

Abstract

Search and rescue operations can greatly benefit from the use of cooperative swarms of autonomous UAVs in order to investigate areas and collect information about the position of a missing person.

In this thesis, UAV swarm algorithms are investigated where collisions are prevented both between agent pairs and between agents and static obstacles. The swarm consists of low-cost collaborative fixed-wing aircraft with communication constraints. A decentralized swarm behavior is first developed when the system is assumed to provide accurate positions of all aircraft. Further, the agents estimate their position by the use of RSSI measurements. All agents are equipped with communication devices and broadcast radio signals and measure the received signal strength in order to estimate the distance to other swarm members. These estimates are further used to develop a multilateration algorithm, where each agent estimates its own position by using distance estimates from a minimum of three nearby agents. By adding a dynamic model of the aircraft kinematics, a more accurate estimation is provided which takes account for false position estimates.

The autonomous swarm is simulated in a 2-D environment in MATLAB. The agents make decisions in real-time, where their movements are controlled by potential fields and pheromone levels. Repulsive potentials are used to prevent collision and attractive potentials are applied to form a cluster of UAVs, such that all members stay within communication range. The swarm is also attracted to unexplored areas of the environment.

When the true UAV positions are provided, the developed potential field algorithm did show promising results in terms of controlling the swarm. No collisions occurred between agent pairs or agents and obstacles. The agents did not go out of bounds and the swarm was robust as it was able to handle the loss of individual members.

For the approach of RSSI based position estimates, further development of the swarm behavior was needed. The receiver sensitivity of the communication devices limits both the maximum distance between agents and their difference in roll angle. When individual failures occurred, or when an obstacle obstructed the path of the swarm, there was not always enough RSSI measurements available to perform the multilateration algorithm. In combination with the dynamic model of the aircraft kinematics, the resulting algorithm produced position estimates with a mean error of approximately 9 meters. No significant difference was found regarding the efficiency of scanning the area when the positions were estimated by RSSI values compared to when the positions were known. However, victims may go undetected when using estimated positions if the position error results in UAVs believing they have visited certain areas they have not yet scanned.

Keywords

Classification system and/or index terms (if any)

Supplementary bibliographical information

ISSN and key title
0280-5316

ISBN

Language
English

Number of pages
1-86

Recipient’s notes

Security classification